Journal of Physics B: Atomic, Molecular and Optical Physics

TOPICAL REVIEW • **OPEN ACCESS**

Charge migration induced by attosecond pulses in bio-relevant molecules

To cite this article: Francesca Calegari *et al* 2016 *J. Phys. B: At. Mol. Opt. Phys.* **49** 142001

View the article online for updates and enhancements.

Related content

- Advances in attosecond science
Francesca Calegari, Giuseppe Sansone, Salvatore Stagira et al.
- Theoretical methods for attosecond electron and nuclear dynamics: applications to the H_2^+ molecule
Alicia Palacios, José Luis Sanz-Vicario and Fernando Martín
- Ultrafast dynamics in isolated molecules and molecular clusters
I V Hertel and W Radloff

Recent citations

- Molecular Modes of Attosecond Charge Migration
Aderonke S. Folorunso *et al*
- Denitsa Baykusheva and Hans Jakob Wörner
- Seunghwoi Han *et al*



IOP ebooks™

Bringing together innovative digital publishing with leading authors from the global scientific community.

Start exploring the collection–download the first chapter of every title for free.

This content was downloaded from IP address 150.244.1.242 on 08/04/2021 at 15:34

OPEN ACCESS
IOP Publishing
Journal of Physics B: Atomic, Molecular and Optical Physics
J. Phys. B: At. Mol. Opt. Phys. **49** (2016) 142001 (25pp)
doi:10.1088/0953-4075/49/14/142001

Topical Review

Charge migration induced by attosecond pulses in bio-relevant molecules

Francesca Calegari[1], Andrea Trabattoni[2], Alicia Palacios[3], David Ayuso[3], Mattea C Castrovilli[1], Jason B Greenwood[4], Piero Decleva[5], Fernando Martín[3,6,7] and Mauro Nisoli[1,2]

[1] Institute for Photonics and Nanotechnologies (IFN)—Consiglio Nazionale delle Ricerche (CNR), Piazza Leonardo da Vinci 32, I-20133 Milano, Italy
[2] Department of Physics, Politecnico di Milano, Piazza Leonardo da Vinci 32, I-20133 Milano, Italy
[3] Departamento de Química, Modulo 13, Universidad Autónoma de Madrid, Cantoblanco, E-28049 Madrid, Spain
[4] Centre for Plasma Physics, School of Maths and Physics, Queens University, Belfast BT7 1NN, UK
[5] Dipartimento di Scienze Chimiche e Farmaceutiche, Università di Trieste and CNR—Istituto Officina dei Materiali, I-34127 Trieste, Italy
[6] Instituto Madrileño de Estudios Avanzados en Nanociencia, Cantoblanco, E-28049 Madrid, Spain
[7] Condensed Matter Physics Center (IFIMAC), Universidad Autónoma de Madrid, E-28049 Madrid, Spain

E-mail: francesca.calegari@polimi.it

Received 3 December 2014, revised 2 May 2016
Accepted for publication 19 May 2016
Published 24 June 2016



Abstract

After sudden ionization of a large molecule, the positive charge can migrate throughout the system on a sub-femtosecond time scale, purely guided by electronic coherences. The possibility to actively explore the role of the electron dynamics in the photo-chemistry of bio-relevant molecules is of fundamental interest for understanding, and perhaps ultimately controlling, the processes leading to damage, mutation and, more generally, to the alteration of the biological functions of the macromolecule. Attosecond laser sources can provide the extreme time resolution required to follow this ultrafast charge flow. In this review we will present recent advances in attosecond molecular science: after a brief description of the results obtained for small molecules, recent experimental and theoretical findings on charge migration in bio-relevant molecules will be discussed.

Keywords: charge migration, attosecond pulses, biomolecules

(Some figures may appear in colour only in the online journal)

1. Introduction

Sudden ionization of a molecule, even a large one, by extreme ultraviolet (XUV) light creates a hole, which has been predicted to migrate on a time scale ranging from few-femtoseconds down to hundreds attoseconds [1–5]. This ultrafast charge migration is driven by the coherent superposition of electronic states generated by the initial pulse. This can be obtained either from a broad pulse, covering several ionization thresholds, or, especially in the case of inner shell ionization, by correlation effects. In both cases the charge is expected to oscillate from one site to another of the molecular backbone (see figure 1) until the interplay between the electronic and nuclear dynamics leads to the final localization of the charge on a specific molecular terminus. Since molecular bonds are more likely to break in places where the hole has migrated, this ultrafast redistribution of the charge could be ultimately



Original content from this work may be used under the terms of the Creative Commons Attribution 3.0 licence. Any further distribution of this work must maintain attribution to the author(s) and the title of the work, journal citation and DOI.

 © 2016 IOP Publishing Ltd Printed in the UK

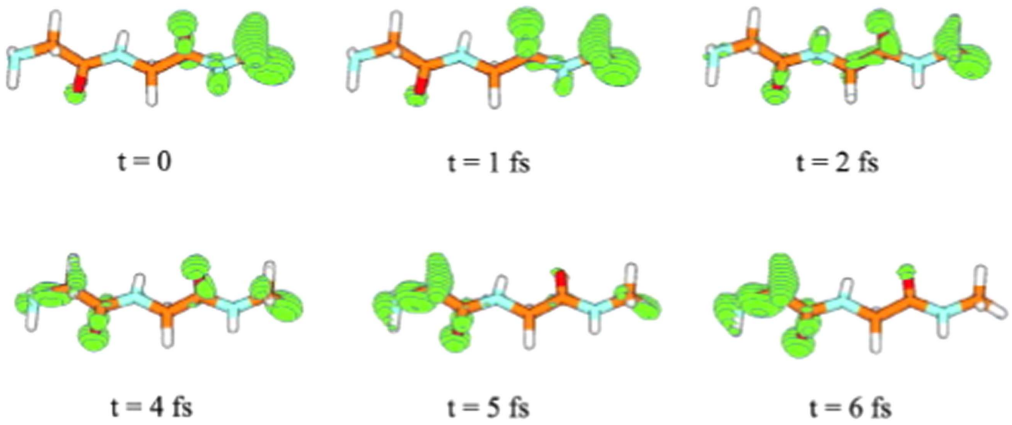


Figure 1. Snapshots of the ultrafast positive-charge migration following inner-valence ionization of the C-terminally methylamidated dipeptide GlyGlyNHCH3. Figure reprinted from [5]. Copyright 2012, with permission from Elsevier.

exploited to obtain a charge-directed reactivity: by acting on the system on the attosecond/few-femtosecond time scale one could in principle control the localization of the charge and consequently induce bond breaking at different molecular sites [6]. The possibility of actively exploring the role of electronic coherences in the photo-chemistry of bio-relevant molecules is of fundamental interest for understanding, and perhaps ultimately controlling, the processes leading to damage, mutation and, more generally, to the alteration of the biological functions of the macromolecule. The interaction of our own biomolecules with ionizing radiation is also exploited in cancer radiotherapy and a better understanding of the mechanisms triggered in the photo-ionization step requires the study of interaction with photons at the molecular level. For the above mentioned reasons, a number of experimental and theoretical works have been recently done to investigate the photo-induced electron dynamics in molecules of increasing complexity. Following this ultrafast dynamics requires extremely high temporal resolution, such that provided by ultrafast laser sources from the femtosecond to the attosecond timescale. Attosecond light pulses are produced in the XUV spectral region exploiting an extremely nonlinear process known as high-order harmonic generation (HHG) [7]. Attosecond science is nowadays a well-established field and the possibility to trace electron dynamics in atoms, small molecules and even solids has been demonstrated [8].

In this review we will investigate ongoing experimental and theoretical efforts aiming to expand the scope of attosecond science for exploration of XUV induced charge dynamics in biologically relevant molecules. We will show that, due to the complex behavior of such molecules exposed to high-energy photons, sophisticated attosecond experiments require accurate theoretical support to extract the intrinsic dynamics of the system from the measured observables. The review is organized as follows: in section 2 we will briefly describe the state-of-the-art of attosecond technology including the XUV generation process and the main spectroscopic techniques based on the use of such ultrafast light transients. Section 3 reports on the advances of attosecond molecular science: after a brief description of the results obtained for small molecules, we discuss recent work on charge migration in aromatic amino acids, which constitute the first experimental evidence of XUV induced pure electron dynamics in bio-relevant molecules. XUV attosecond spectroscopy of biomolecules requires the production of molecules in the gas phase or at a vacuum interface. In section 4 we will revise the main techniques for liberating molecules in gas phase, which have enabled a range of species to be produced in ionic or neutral form. Finally, the most recent theoretical advances in describing the charge dynamics induced by XUV attosecond pulses in bio-relevant molecules are reported in section 5.

2. Attosecond technology

The possibility of using attosecond pulses for the investigation of ultrafast electronic processes in atoms, molecules, nanostructures and condensed matter is strictly related to the development of experimental schemes for reliable generation of sub-femtosecond pulses [8–10]. In the last decade new experimental techniques have been proposed, which require the generation of attosecond pulses with proper characteristics in terms of pulse energy, photon energy tunability and polarization state. For measurements in combination with femtosecond pulses, pulse energies larger than a few tens of picojoules are sufficient, while for attosecond-pump/attosecond-probe applications hundreds of nanojoules are required [11]. The polarization state of the XUV pulses can be a very interesting experimental tool for the investigation of various physical processes. In particular, circularly polarized XUV pulses have important applications for the investigation of ultrafast electronic processes in chiral species and in magnetic materials, to name just a few examples [12–14].

The production of sub-femtosecond pulses generally relies on the process of HHG in noble gases [7]. When an ultrashort pulse is focused in a gas at intensities of the order of 10^{13}–10^{14} W cm^{-2}, the Coulomb potential experienced by the outer shell electrons is strongly modified, with the formation of a potential barrier through which an electron can escape by

tunnel ionization. This highly nonlinear process gives rise to the generation of an ultrashort electron wavepacket moving in the continuum, perfectly synchronized with the laser field. The freed electron is subsequently accelerated by the driving field, thus acquiring kinetic energy with a maximum value $\mathcal{E}_{k,\max} \approx 3.17U_p$, where U_p is the ponderomotive energy, i.e. the mean kinetic energy of an electron in an oscillating laser field, which turns out to depend on the central wavelength, λ, and peak intensity, I, of the excitation laser: $U_p \propto \lambda^2 I$. The generation of an attosecond electron wavepacket is particularly important for the applications since it offers the possibility to combine an extreme temporal resolution, related to the strongly nonlinear dependence of the tunneling ionization process on pulse intensity, to an extreme spatial resolution, related to the de Broglie wavelength of the ejected electron. For typical energies of this electron the corresponding de Broglie wavelength is of the order of a few Ångströms. Such extreme spatial resolution is at the heart of molecular tomography, which has been proven to be able to reconstruct the molecular orbitals of a few molecules [15–17].

In the case of an excitation field with linear polarization, the freed electron can return to the parent ion and recombine to the ground state: the energy acquired by the recolliding electron in the laser field is emitted in the form of an ultrashort photon pulse in the XUV spectral range. Since tunnel ionization produces short electron wavepackets at each field crest of the driving pulse, the above three-step mechanism (tunnel ionization, motion in the continuum, recollision) leads to the generation of a train of sub-femtosecond XUV pulses separated by half optical cycle of the fundamental radiation. In the spectral domain this corresponds to the generation of the high-order (odd) harmonics of the driving frequency. Due to the very low conversion efficiency of the harmonic generation process, in the range 10^{-4}–10^{-6}, the energy of the attosecond pulses is generally quite low, in the range between a few hundreds of picojoules and a few nanojoules. A number of schemes have been demonstrated for the generation of attosecond pulses with energy in the microjoule range [11], mainly based on the use of the loose-focusing geometry, where the excitation pulses are focused in a long gas cell by using long focal length optics. Recently, high-energy attosecond pulses have been used in XUV-pump/XUV-probe measurements for the investigation of nuclear and electronic dynamics in H_2 molecules [18, 19]. In this review we will concentrate on the application of low-energy attosecond pulses in molecular physics, in the form of attosecond pulse trains and isolated attosecond pulses.

Several techniques can be exploited to confine the harmonic generation process to a single event in order to produce isolated attosecond pulses, based on the use of amplitude gating or temporal gating schemes (for a comprehensive review see [10, 11]). For example, a short gate for harmonic generation can be produced by taking advantage of the strong dependence of harmonic conversion efficiency on the polarization state of the driving pulse. As first proposed in 1994, a driving pulse characterized by almost linear polarization in a very short temporal window around the peak of the pulse and elliptical polarization on the leading and trailing edges, is an ideal source of isolated attosecond pulses [20]. A very simple experimental setup to produce this exotic polarization state makes use of two birefringent plates [21]. This technique, called polarization gating, was experimentally tested in 2006 [22, 23] and it is now used in various laboratories.

One of the major limitations of the above mentioned gating technique is a strong reduction of the produced XUV photon flux (typically few hundreds pJ per pulse). Low-density targets, such as biorelevant molecules in gas-phase, require high XUV photon flux to achieve sufficient statistics. In 2010 Ferrari *et al* demonstrated a new gating approach based on sub-cycle ionization dynamics for the generation of isolated attosecond pulses at the nJ-energy level. This method is based on the combination of a high-intensity few-optical cycles driving pulse and a low-IP generating medium (e.g. xenon): the rapid increase of ionization leads to efficient population depletion over the first few half-cycles thus suppressing HHG for all later half-cycles. By using this approach isolated attosecond pulses with temporal duration down to 155 as and an energy on target of 2.1 nJ have been generated [24].

A completely different experimental technique for the generation of isolated attosecond pulses has been reported more recently by Hassan and coworkers [25]. Attosecond optical pulses have been synthesized in the visible and ultraviolet spectral region by coherent combination of pulses in various spectral regions over more than two optical octaves [26, 27]. Ultrabroad spectral broadening was obtained by propagating femtosecond pulses in an hollow-core fiber filled with neon [28]. The beam at the output of the fiber was first divided into four beams in four different spectral regions, ranging from near-infrared (NIR) to deep ultraviolet. After compression of individual pulses in a four-arm interferometer, obtained by using properly designed chirped mirrors, the four pulses were then spatially and temporally superimposed in order to generate a single ultra-broadband pulse. Pulses as short as 380 as have been reported, with an energy up to about 50 μJ [25].

Various experimental techniques have been implemented to take advantage of the extreme temporal resolution of the attosecond pulses. Particularly important is the attosecond streaking scheme, which is extensively used for the temporal characterization of the attosecond pulses [29]. It is based on the concept of attosecond streak camera [30]. The attosecond pulse is focused on a gas; the generated photo-electrons are then accelerated in a strong NIR field, which is a small portion of the driving pulse, suitably delayed with respect to the attosecond pulse. Upon measuring the evolution of the kinetic energy of the photoelectrons as a function of the delay between the XUV and the NIR pulses it is possible to retrieve the temporal characteristics of the attosecond pulse [31]. This technique can be also used to investigate ultrafast electron dynamics in atoms and solids. For example, in the case of condensed matter, the measurement of the streaking traces of core-level (4f) and conduction-band electrons produced in tungsten crystals exposed to attosecond pulses, allowed the measurement of a delay in photoemission of the above two classes of electrons of ~100 as [32].

In the case of trains of attosecond pulses the measurement of the kinetic energy of the photoelectrons produced by the attosecond pulses in the presence of a weak NIR field, as a function of the temporal delay between the XUV and NIR pulses, was the very first application of an attosecond experimental technique for the measurement of the duration of sub-femtosecond pulses [33]. The technique is called reconstruction of attosecond beating by interference of two-photon transitions. In this case the spectrum of the photoelectrons presents discrete peaks, which correspond to transitions induced by single-photon absorption of XUV harmonics, separated by $2\hbar\omega$, where ω is the frequency of the NIR radiation. When the XUV and NIR pulses are temporally overlapped, one NIR photon can be absorbed or emitted (in the case of weak NIR pulses), thus giving rise to additional peaks in the photoelectron spectra at $\pm\hbar\omega$ with respect to the peaks produced by the XUV harmonics, whose amplitude is periodically modulated versus XUV-NIR temporal delay. From this modulation it is possible to measure the relative phases of consecutive harmonics and to retrieve the duration of each XUV pulse in the train. The same technique has been also used to measure the delay in photoemission from noble gas atoms [34] and from metal surfaces [35].

Another experimental approach, still belonging to the class of attosecond photoemission spectroscopy, is based on the measurement of ion yields as a function of the temporal delay between an attosecond pump pulse and a femtosecond probe pulse. This technique was employed by Uiberacker and coworkers for the first real-time measurement of light-field-induced electron tunneling in neon [36]. Clear signature of electron tunneling was obtained by measuring the evolution of the number of Ne^{2+} ions produced by the interaction of 5 fs NIR pulses with neon atoms ionized by isolated attosecond pulses. Angle-resolved measurements of ions vs pump-probe delay have been also successfully employed in pump-probe experiments on small molecules using isolated attosecond pulses [37, 38] or trains of attosecond pulses [39–41]. More recent advances on attosecond molecular spectroscopy will be discussed in section 3.

A different class of experimental techniques is based on all-optical schemes. A first example is given by attosecond transient absorption spectroscopy, which has been implemented with both isolated pulses and trains of pulses. In this case the attosecond pulses are used as probe pulses: their photon spectra are measured as a function of the temporal delay between the femtosecond-pump and the attosecond-probe pulses. This technique was first applied in 2010 to the investigation of attosecond time-resolved autoionization of Argon [42], for real-time observation of valence electron motion in Krypton [43], and for the time reconstruction of a two-electron wave packet in Helium [44]. More recently, attosecond transient-absorption spectroscopy has been used to investigate ultrafast processes in solids [45–47]. Another experimental scheme based on optical measurements is high harmonic spectroscopy (HHS), which will be presented in detail in section 3.3. This technique is based on the detection of photons emitted during the recollision process leading to harmonic generation. As a direct consequence of the physical processes at the heart of HHG, the emitted spectrum carries information on both the ionization and the recollision processes as well as on the structure of the ionized medium and on any temporal evolution of the hole left in the parent ion between ionization and recombination events.

3. Advances in attosecond molecular science

Dynamical processes in molecules occur on an ultrafast temporal scale, ranging all the way from picoseconds to femtoseconds when considering structural changes and down to attoseconds when dealing with electrons. In the last decade, attosecond photoemission spectroscopy has been proven to be an excellent tool for investigating ultrafast electron dynamics induced in gas-phase molecules [6]. Isolated attosecond pulses have been used in combination with waveform controlled NIR pulses with the aim of controlling charge localization after sudden ionization of H_2 (D_2) molecules [37]. More recently, the dissociative ionization dynamics of N_2 has been measured with attosecond time resolution and crucial information on the shape of the potential energy curves (PECs) involved in the dissociative process has been retrieved [38]. By extending the same experimental approach to the study of biologically relevant molecules, the first evidence of charge migration in an aromatic amino acid was achieved [48–50]. Complementary to photoemission spectroscopy, HHS was successfully demonstrated to be a powerful technique to obtain substantial information on the molecular orbitals involved in the HHG process for small molecules. Very recently this approach has been extended to a more complex molecule (iodoacetylene) and charge migration has been evidenced to occur along the linear molecule on a sub-femtosecond time scale [51]. These experiments will be discussed in detail in the following subsections.

3.1. Attosecond spectroscopy of ultrafast molecular dynamics

In 2010 Sansone *et al* performed the first pump-probe measurement, using isolated attosecond pulses, to suddenly ionize H_2 (D_2) molecules and investigate the photo-induced ultrafast electron dynamics. The angular momentum distribution of the produced H^+ (D^+) fragments was measured with a velocity map imaging spectrometer (VMI) as a function of the delay between the attosecond pump pulse (energy range 20–40 eV) and the 6 fs, CEP-stable NIR probe pulse. The experiment revealed that dissociative ionization of H_2 (D_2) molecules induced by the combination of isolated XUV attosecond pulses and NIR pulses inevitably leads to electron localization. This process has been identified through the asymmetry parameter, which is evaluated from the difference in the numbers of H^+ (D^+) ions arriving on the left-hand and right-hand sides of the detector. In the kinetic energy range between 2 and 10 eV the asymmetry parameter was found to exhibit sub-cycle oscillations as a function of the delay between the XUV and the NIR pulses. This asymmetry is the result of a coherent superposition of gerade and ungerade states, and the relative phase between the two states results in

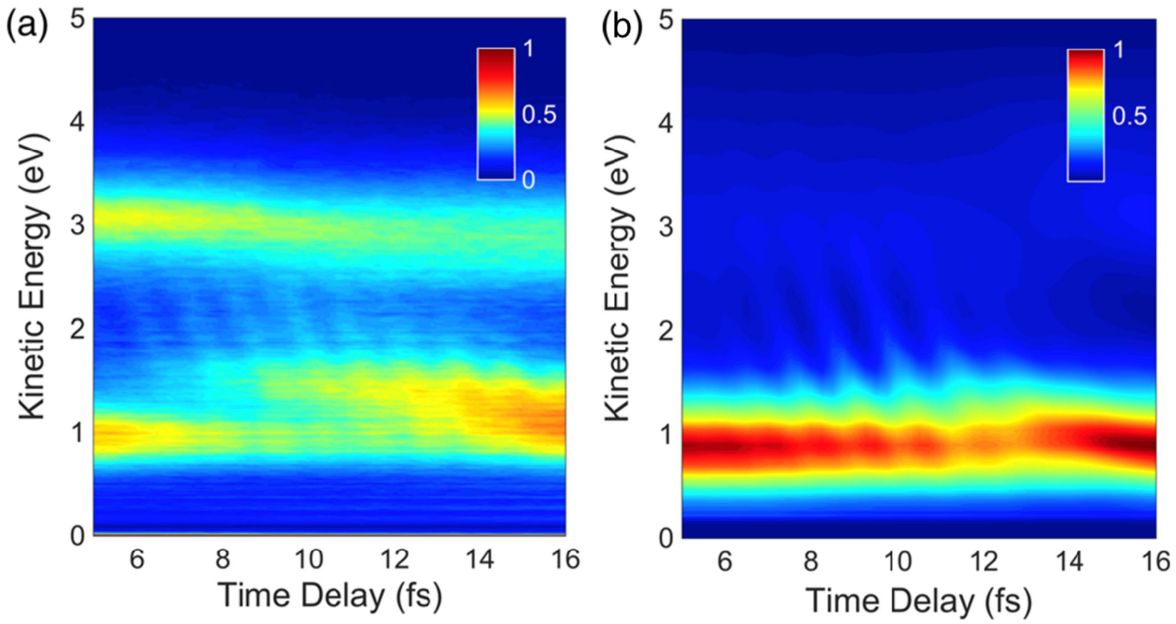


Figure 2. (a) Time-dependent N^+ kinetic energy spectra acquired within the pump-probe delay interval 5–16 fs.(b) Simulation of time-dependent N^+ kinetic energy spectra in the same delay interval. Figure reprinted from [38]. Copyright 2015, with permission from Elsevier.

electron localization on one atom or the other of the molecule [37]. One year after this important result, a similar experiment was performed by Kelkensberg *et al*: in this case a moderately intense NIR pulse (3×10^{13} W cm^{-2}) was used in combination with an XUV attosecond pulse train. While in the experiment described above the attosecond pulses were used to initiate electron dynamics which were subsequently probed by the NIR field, in this case the NIR pulse was used to influence the electronic states that are accessed in photoionization of H_2 by the APTs and a time dependent polarization of the molecule was measured [39].

These pioneering works, performed on the simplest molecule (H_2), opened the way to the investigation of more complex molecules. Indeed, in the past few years important experiments were successfully performed on multi-electron diatomic molecules and small polyatomic molecules. Among them, attosecond pulse trains in combination with NIR femtosecond probe pulses were used to investigate the dissociative dynamics and the vibrational motion in the binding potentials of O_2^+ [40, 52], while narrow-band XUV excitation was exploited to study autoionization in O_2 [53]. A slightly different method, exploiting waveform-controlled high-intensity NIR pulses, was used to investigate ultrafast electron dynamics in CO [54]. In 2013 Neidel *et al* reported the observation of attosecond time-scale electron dynamics in various molecules (N_2, CO_2, and C_2H_4). In this case the time-dependent dipole induced by a NIR laser field was probed by measuring the time-dependent variations of the parent molecular ion yield in the ionization by an attosecond pulse train [41].

Attosecond spectroscopy was also extensively used for the study of the dissociative dynamics of N_2 following XUV photoionization. Indeed, molecular nitrogen is the most abundant species in the Earth's atmosphere, and investigating the ultrafast dissociative mechanisms triggered by the absorption of XUV photons (leading to the production of N atoms and N^+ ions in the upper layers of the atmosphere) is of prime importance for understanding the radiative-transfer processes. The use of attosecond pulse trains in combination with VMI spectroscopy has allowed the measurement of autoionization dynamics in N_2^+ [55]. The time-to-internuclear distance mapping obtained in this experiment has been demonstrated to be a precise clock which measures, with femtosecond temporal resolution, when autoionization starts to be an energetically allowed process. Dissociative ionization of N_2 was further studied in a recent work applying femtosecond time-resolved photoelectron and photoion spectroscopy using a tabletop XUV time-compensating monochromator [56]. Although attosecond spectroscopy allows one to achieve extreme time resolution, the intrinsic broadband nature of the attosecond excitation inevitably leads to the superposition of a number of electronic states. As a consequence, the investigation of electronic and nuclear dynamics following ionization of even small molecules such as N_2 by attosecond pulses is considered a challange. Therefore, experimental results need to be guided by theoretical models taking into account a precise description of the PECs and couplings, including all the electrons of the system. Since this is generally difficult, we could assert that molecular attosecond science of such multi-electron systems is still in its infancy. Recently, Trabattoni *et al* demonstrated that isolated attosecond pulses can be exploited to access the dissociative ionization dynamics of molecular nitrogen with extremely high temporal resolution and, with the support of a sophisticated theoretical model, precise information on the shape of the PECs involved in the dissociative mechanism have been achieved [38]. In this experiment, molecular nitrogen was photoionized by the combination of a sub-300-as

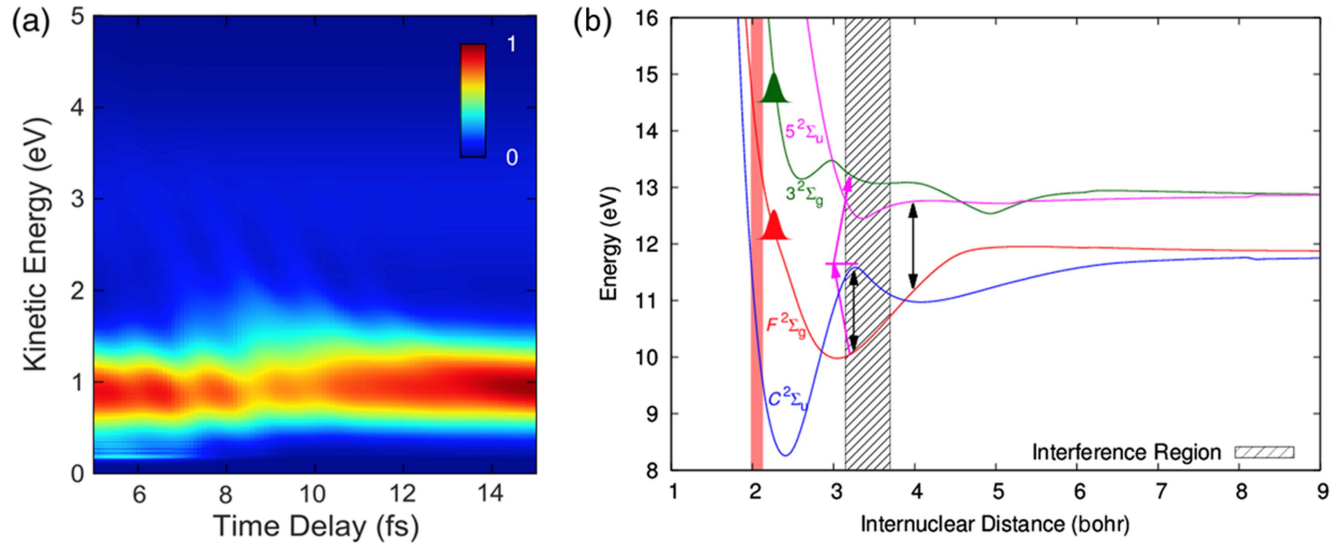


Figure 3. (a) Simulation of time-dependent N^+ kinetic energy spectra with the simplified model. (b) Four-state model, where the $F^2\Sigma_g$, $3^2\Sigma_g$, $C^2\Sigma_u$ and $5^2\Sigma_u$ states were considered. Figure reprinted from [38]. Copyright 2015, with permission from Elsevier.

attosecond pump pulse (energy range between 16 and 50 eV) and a waveform-controlled sub-4 fs NIR probe pulse.

As for the experiment performed in [55], the 3D momentum distribution of the N^+ ions was measured with a VMIs as a function of the delay between the XUV pump pulse and the NIR probe pulse. Figure 2(a) shows the kinetic energy spectrum of N^+, obtained by integration of the angular distribution over a small angle along the laser polarization axis, in the pump-probe delay range between 5 and 16 fs. Two main features can be observed: (i) the depletion of the signal at 1 eV occurring 8 fs after the zero delay, (ii) the appearance of a fast modulation in the same delay range, with a periodicity of 1.22 fs. Furthermore the modulation shows an energy-dependent phase, resulting in a tilt of the fringes.

To understand the role of the manifold of excited states in the features observed in the pump-probe delay scan, a sophisticated theoretical model was developed. The time-dependent Schrödinger equation (TDSE) has been solved for a set of 616 diabatic excited states of N_2^+, taking into account the couplings induced by the NIR probe pulse. TDSE is solved by using a split-operator technique in combination with fast-Fourier techniques. In this methodology, the nuclear wave packet (NWP) is discretized on a grid of internuclear distances and the propagation of the wave packet is performed on a set of coupled electronic states (including nonadiabatic and dipole couplings) calculated on the same grid. Figure 2(b) shows the calculated N^+ kinetic energy spectrum as a function of the pump-probe delay, obtained by considering the same parameters of the experiments. As can be seen from this figure, a very good agreement has been achieved between theory and experiment. However, the full calculation does not allow the role of the individual PECs in the measured dynamics to be extracted. For this reason a simple model has been developed, for which only four states were considered, namely the $F^2\Sigma_g$, $3^2\Sigma_g$, $C^2\Sigma_u$ and $5^2\Sigma_u$ states. Figure 3(a) shows the result of the 4-state model: also in this case the main features observed in the experiments are reproduced. The simplified model allows one to disclose the physical mechanisms occurring in the molecule as schematically represented in figure 3(b): the depletion of the signal around 1 eV is related to resonant single-photon transitions from the $F^2\Sigma_g$ state to the $5^2\Sigma_u$ state and from the $F^2\Sigma_g$ state to the $C^2\Sigma_u$ state induced by the NIR probe pulse (black double-headed arrows in the figure). The measured delay of 8 fs corresponds to the time required by the NWP to reach the single-photon transition point. Additionally, the ultrafast periodic modulation results from the interference between the initial population of the $3^2\Sigma_g$ state and the population transferred to the $3^2\Sigma_g$ state from the $F^2\Sigma_g$ state via a two-photon transition using the $5^2\Sigma_u$ state as a virtual intermediate state (magenta single-headed arrows). The tilt in the fringes is due to the dispersion of the components of the NWP while traveling along the PECs. This time-versus-energy dependence carries crucial and precise information about the quantum path followed by the NWP, namely the shape of the PECs involved in the interference. It can be shown that by artificially changing the slope of the $3^2\Sigma_g$ state the resulting tilt in the fringes dramatically changes and the agreement with the experimental data is lost.

This result demonstrates that the attosecond experiments serve as a benchmark for a complex theoretical model, which also provides accurate values for the dissociative ionization yields revealing that realistic modeling of nitrogen chemistry in planetary atmospheres should also incorporate the presence of nitrogen atoms or ions in various excited states, which are likely to have a different reactivity.

Finally, it is worth mentioning that attosecond molecular spectroscopy has been recently extended to polycyclic aromatic hydrocarbons (PAHs), which account for 10% of the elemental carbon in galaxies. In the experiment, a typical fs XUV pump—fs NIR probe arrangement has been used and the mass of the produced photo-fragments has been measured as a function of the pump-probe delay. A rapid

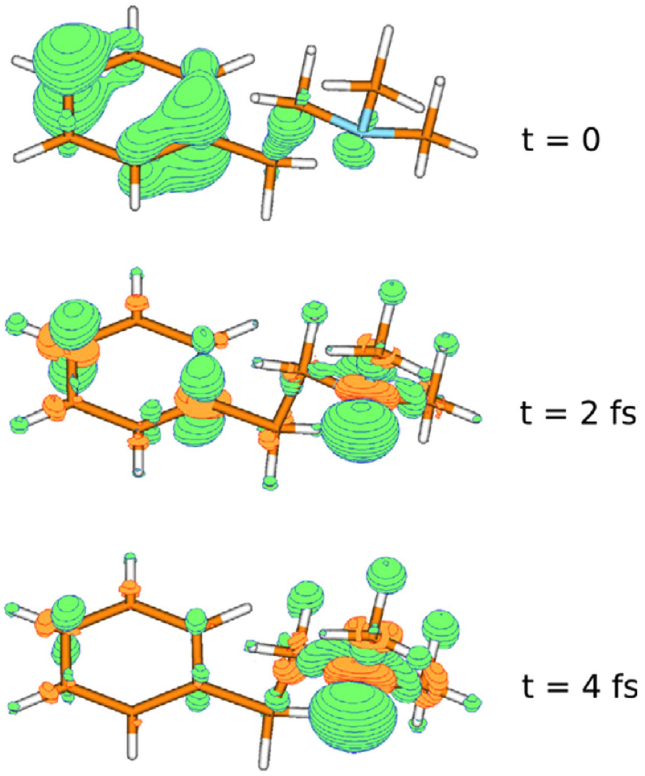


Figure 4. Time evolution of the 3D-hole density of PENNA calculated for the geometry with the C_1–C_2 bond elongated by 20 pm. Reprinted from [59]. Copyright 2008, with permission from Elsevier.

decay of a dicationic signal has been identified for naphthalene, anthracene, pyrene and tetracene, which has been assigned to a very fast relaxation of the excited cationic states following XUV ionization due to non-Born–Oppenheimer couplings [57]. These experimental results demonstrate that the complexity of the molecular targets investigated by attosecond spectroscopy has rapidly increased and, as will be shown in the following subsection, important outcomes for photochemistry and photobiology are forseen.

3.2. Electron dynamics in bio-relevant molecules

The interaction of large polyatomic molecules with light is likely to initiate a charge transfer mechanism, which plays a crucial role in a number of chemical and biological processes. The term *charge transfer* traditionally indicates a transfer of the charge along the molecular backbone mediated by the nuclear motion, which occurs in several tens of femtoseconds. However, many theoretical works indicated that after the sudden removal of an electron in a large molecule the positive charge can migrate throughout the system solely driven by electronic correlations on a sub-femtosecond time scale. This ultrafast process has been termed *charge migration*. Even before the advent of attosecond sources, a pioneering experiment in this direction was performed by Lehr *et al* in 2-Phenylethyl-N,N-dimethylamine (PENNA) as a model system for the investigation of nonresonant downhill charge

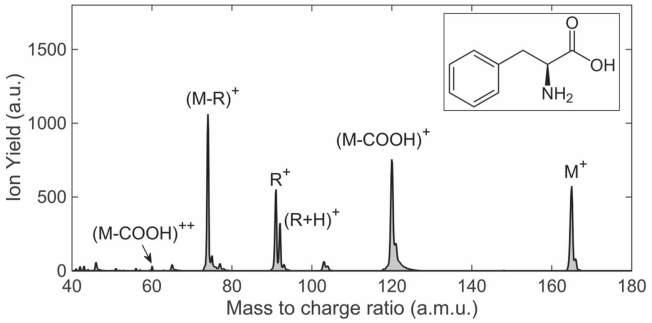


Figure 5. Mass spectrum of phenylalanine obtained by photoionization by XUV pulses with photon energy in the range 16–40 eV. Inset: molecular structure.

transfer in peptides [58]. In this work, after local ionization of the phenyl chromophore site, charge transfer to the N-terminal (amine group) has been demonstrated to occur in 80 ± 28 fs using a pump-probe scheme. Subsequently, a theoretical work by Lünneman *et al* assigned the measured time of 80 fs to an upper limit for the duration of the charge transfer between the amine group and the phenyl chromophore. Indeed, charge migration between the two molecular sites has been predicted to occur in 4 fs (see figure 4), revealing that several oscillations are required until the charge is finally trapped at the N-moiety due to the elongation of the C_1–C_2 bond [59].

Following the development of attosecond sources, it was proposed to initiate and track in real time the charge migration process resulting in rapid oscillations between two molecular sites. However, as it will be shown in section 5, the use of attosecond sources inevitably leads to the excitation of electronic coherences due to the large bandwidth of attosecond pulses. Thus the term charge migration, initially assigned to pure correlation effects, has been extended to charge dynamics induced by the coherent superposition of singly excited cationic states originated by sudden ionization. The possibility to trigger ultrafast charge dynamics via electronic coherences has stimulated discussions about future applications of attosecond technology to obtain a charge-directed reactivity. The investigation of pure electron dynamics initiated by sudden excitation or ionization of biomolecular building blocks is currently of great interest as this process could be seen as the precursor for a number of biologically relevant processes, e.g. DNA strand breaks, thymine base dimerization [60], protein–protein cross-links [61, 62].

In 2012 Belshaw and co-authors performed the first experiment exploiting the use of attosecond pulses to initiate ultrafast charge dynamics in a biologically relevant molecule, namely the aromatic amino acid phenylalanine [48]. In the experimental setup laser-induced acoustic desorption (LIAD) [63] was used to produced a clean plume of neutral molecules which have been irradiated by a 1.5 fs XUV pump pulse with a photon energy in the range 16–40 eV, followed at a controllable delay time by a 6 fs NIR (500–950 nm, NIR) probe pulse with an intensity of 8×10^{12} W cm^{-2}. The parent and fragment ions produced were then extracted into a linear time-of-flight device for mass analysis. Figure 5 shows the

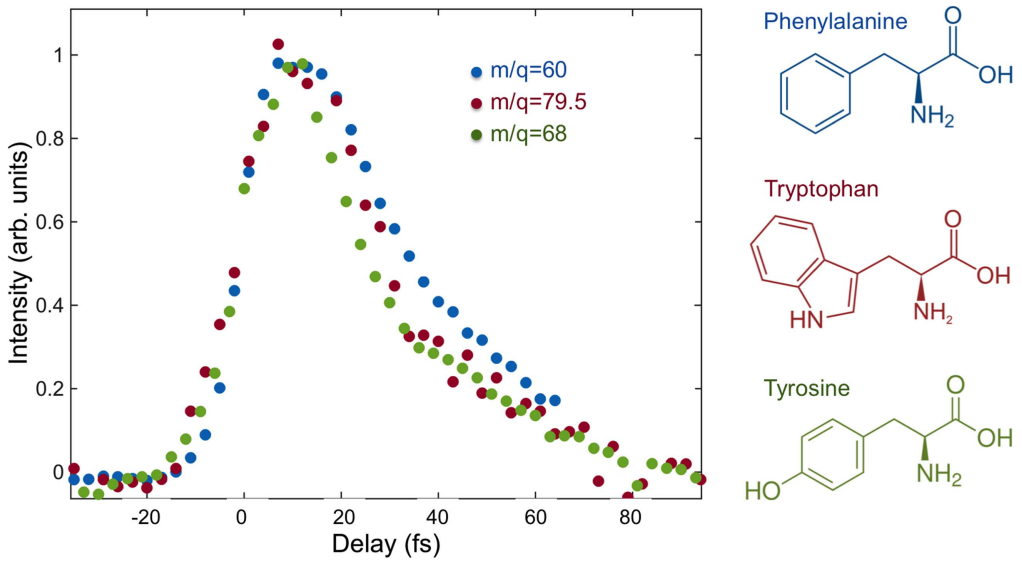


Figure 6. Doubly charged immonium ion yield as a function of the XUV pump NIR probe delay for phenylalanine (blue dotted line), tryptophan (red dotted line) and tyrosine (green dotted line).

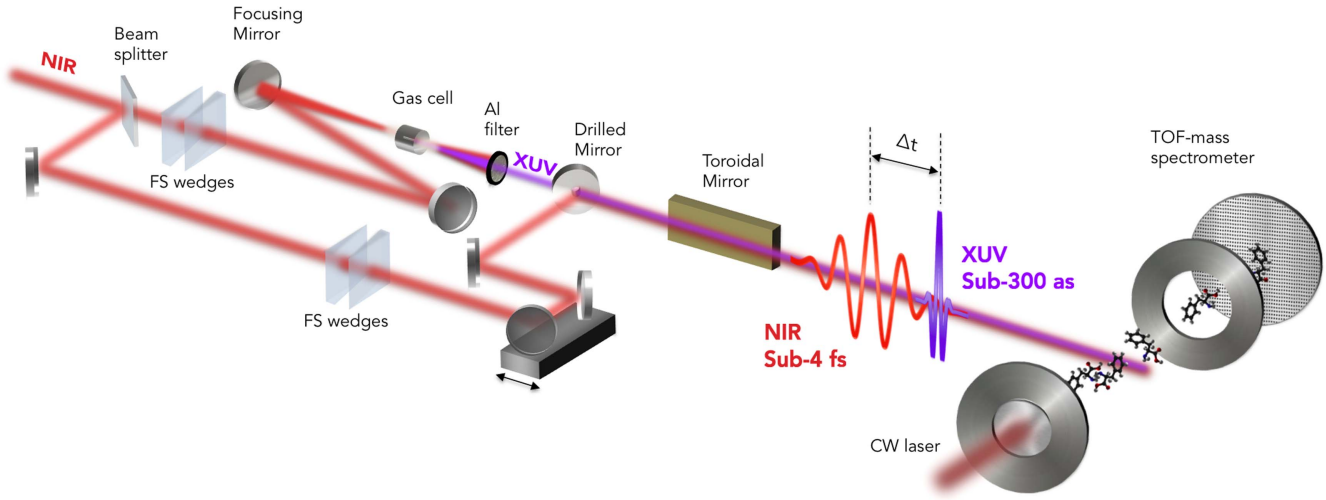


Figure 7. Scheme of the attosecond setup used to initiate and track electron dynamics in phenylalanine.

structure of the amino acid and a typical mass spectrum produced by photoionization using the XUV pulses. As can be seen from this figure, a wide range of fragment ions are produced by the interaction with the XUV light: the main contributions correspond to the parent ion M^+ (165), the immonium ion (M-COOH = 120) resulting from the loss of the carboxyl group, and fragments resulting from the breakage of the C_α–C_β bond with charge residing on the amine (M−R = 74) or phenyl groups (R = 91, R + H = 92). For some of the singly charged fragments (65, 77, 91, 103) an increase for positive delays with a time constant of 80 ± 20 fs has been measured. This temporal evolution has been attributed to an internal conversion process into the π_1 state of the phenyl radical cation following initial ionization of a different orbital by the XUV pulse. A preliminary indication of ultrafast charge dynamics occurring in the molecule has been identified already in this experiment, where a rapid decay in the doubly charged immonium ion (m/q = 60) yield has been measured. Subsequent measurements performed in tryptophan and tyrosine revealed that the ultrafast relaxation dynamics identified for phenylalanine is present in all the aromatic amino acids. Figure 6 shows the doubly charged immonium ion yield measured as a function of the XUV pump NIR probe delay for phenylalanine (m/q = 60), tryptophan (m/q = 79.5) and tyrosine (m/q = 68): the extracted decay time is 25 fs for phenylalanine, 23 fs for tryptophan and 20 fs for tyrosine.

More recently, the same experiment performed in phenylalanine with a higher temporal resolution has allowed a sub-4.5 fs modulation of the dication yield to be identified, which originates from electronic beatings between different functional groups of the amino acid [49, 50]. A schematic of the experimental setup is reported in figure 7: charge migration was initiated by isolated sub-300 as pulses, with photon energy between 15 and 35 eV and it was subsequently probed by sub-4 fs, waveform-controlled NIR pulses. In this case,

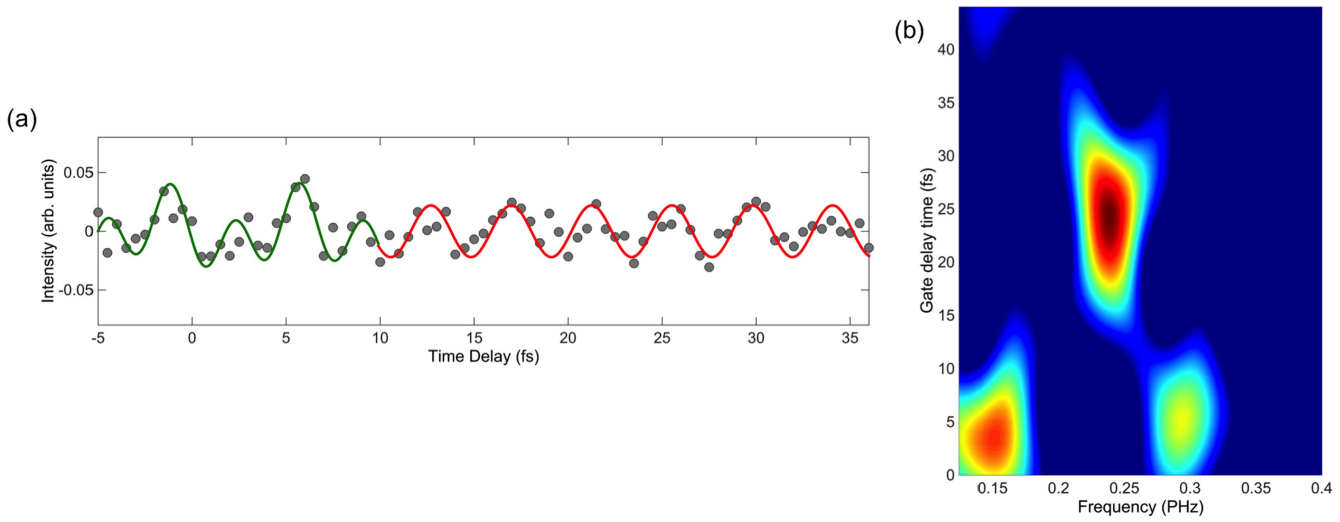


Figure 8. (a) Yield of doubly charged immonium ion ($m/q = 60$) as a function of pump-probe delay obtained after subtraction of the 25 fs dynamics. (b) Time-dependent Fourier analysis of the experimental data.

phenylalanine molecules were produced in the gas phase by evaporation from a thin metallic foil heated by a continuous wave (CW) laser. The metallic foil was integrated in the repeller electrode of the time-of-flight mass spectrometer and the mass of the produced ions was analyzed as a function of the delay between the XUV-pump and NIR-probe pulses. Charge migration was evidenced in phenylalanine as a fast modulation of the dication yield. This periodic modulation (figure 8(a)) can be clearly observed after subtraction of the 25 fs dynamics, resulting in clean oscillations with different periodicities. Figure 8(b) shows the time-dependent Fourier analysis of the experimental data, which revealed the presence of two frequencies around 0.12 and 0.29 PHz in the time-delay interval 0–10 fs, and a single frequency around 0.24 PHz at longer pump-probe delays (10–36 fs). The frequencies retrieved from the time-dependent Fourier analysis for the two time-delay intervals have been used to fit the experimental data, resulting in the green and red sinusoidal curves reported in figure 8(a). The main beating frequency of 0.24 PHz corresponds to an oscillation period of 4.3 fs, shorter than the vibrational response of the molecule, thus indicating the presence of a pure electronic process. Numerical simulations have been performed (details in section 5) in order to reproduce the temporal evolution of the electronic wave packet created by the attosecond pulse. The theoretical results indicate that charge migration is originated from the coherent superposition of a number of electronic states. In particular, the 4.3 fs oscillations have been mainly assigned to periodic charge migration from the amine functional group to the carboxylic group and back of the amino acid.

3.3. High-order harmonic spectroscopy: increasing the target complexity

HHG is a well established technique used to upconvert a low-frequency ultra intense laser field into high-energy radiation, ranging from VUV to soft x-rays [64]. As already mentioned in section 1, this process can be fully described with a semiclassical three-step model [7], in which a valence electron is tunnel ionized by an intense laser pulse, and after being accelerated in the continuum it recombines with the parent ion by emitting an XUV photon. Since the wavelength of a typical recollision electron matches the size of the valence electron orbitals, this process provides extreme temporal (sub-femtosecond) and spatial (Ångström) resolution. If HHG occurs in molecules, the evolution of the parent molecular cation (vibrational and rotational dynamics as well as hole migration) can be probed by the recolliding electron, where the time between ionization and return can be viewed as the pump-probe delay. The control of the pump-probe delay is intrinsically included in the HHG process since an individual XUV spectrum contains a broad range of energies corresponding to different time intervals spent by the electron in the continuum. Following this idea, in 2006 Baker *et al* demonstrated that ultrafast molecular dynamics can be monitored with attosecond time resolution by chirp-encoded recollision (PACER) technique and both nuclear dynamics in H_2^+ and structural rearrangement in CH_4 and CD_4 have been measured [65].

One of the fundamental challenges in applying HHS to resolve electron and nuclear rearrangement is the need to decouple temporal and spatial information encoded in the HHG spectrum, including the electron and nuclear dynamics. This requires characterization of the basic stages of the interaction: ionization, electron–hole dynamics, and radiative electron–hole recombination. For this reason, an advanced scheme for multi-dimensional HHS has been developed, based on using phase-locked multi-color laser fields [66]. In such fields, the electron trajectories can be shaped within one optical cycle by controlling the relative phases and polarizations between the different fields. This enables one to manipulate the vectorial properties of the electron-cation recombination process. Scanning the relative delay between the different colors reveals the multidimensional nature of the interaction. In 2012 Sharif *et al* implemented this general idea by performing HHG in CO_2 using the combination of an intense NIR laser pulse with its weak and perpendicularly

polarized second harmonic field [67]. By measuring the emitted harmonic spectrum as a function of the relative delay between the two-color components, the authors have been able to extract the time required by the electron to tunnel ionize. The contribution from two molecular orbitals (highest occupied molecular orbital (HOMO) and HOMO-2) has been identified and a precise estimation of the relative ionization delays has been obtained. This result is particularly important, since it underlines the capability of independently accessing the single steps of the generation process, and it opens new perspectives in the investigation of multi electron contributions in the framework of strong-field tunneling ionization.

Since the harmonic spectrum originates from the interference between the recolliding electron wavepacket and the parent orbital, it also encodes detailed information on the electronic structure of the target. This property of the HHG process was successfully used to both probe multi electron rearrangements induced by strong field ionization [68–70], and to tomographycally reconstruct molecular orbitals. The first experiment of molecular tomography was proposed and demonstrated in 2004, with the retrieval of the HOMO of N_2 [15]. In 2011 a generalization of the tomographic technique based on a self-referencing approach has allowed the tomographic reconstruction of a more complex molecules, namely CO_2 [17], and afterwards it has been successfully extended to other molecules including N_2O and acetylene [71].

Most of the HHS experiments rely on the alignment/orientation of the molecular ensemble with respect to the driving laser polarization axis, this aspect constitutes one of the major limitations of the technique which has been extensively applied only to small (and often linear) molecules. Recently, the encouraging results obtained by Cireasa and coworkers for chiral molecules have opened new important perspectives for the extension of HHS to bio-relevant molecules [72]. In this experiment, HHG was performed in randomly oriented chiral molecules (epoxypropane and fenchone) to probe chiral interactions on the sub-femtosecond timescale. In order to obtain an extended HHG spectrum from such low-IP molecules, an IR laser (1.8 μm) was used to drive the generation process. The harmonic spectrum was measured as a function of the ellipticity ϵ of the driving field. In achiral species, the HHG yield maximizes for $\epsilon = 0$ and it decays in a symmetric way as ϵ increases: this strong dependence of HHG on ellipticity is due to the lateral displacement acquired by the liberated electron which eventually misses the paren ion. In contrast, HHG in chiral molecules shows an asymmetric dependence on ϵ (elliptical dichroism). Figure 9 shows the value of ϵ which provides the maximum signal for each harmonic order (maximizing ellipticity) for epoxypropane (panel (a)) and fenchone (panel (b)). Red (blue) traces correspond to *S*- (*R*-) enantiomers while the gray line shows a non-chiral reference (xenon). As can be seen from this figure, the dependence is essentially flat for fenchone, while it exhibits a complex dependence for epoxypropane with a maximum/minimum for harmonic 41. In order to understand this result, the contribution to the harmonic emission from different channels needs to be considered: *direct channels* (ionization from and recombination with the same state) or

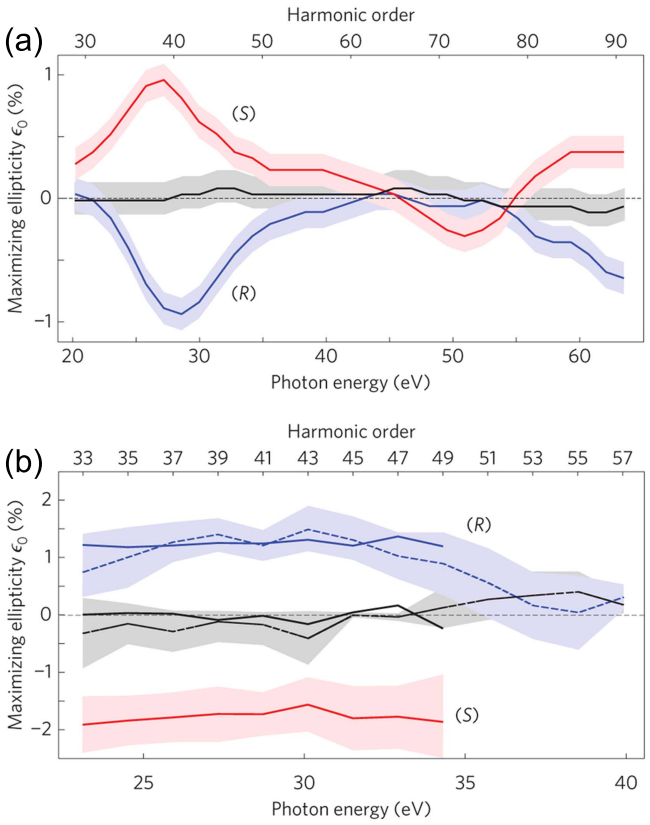


Figure 9. Maximizing ellipticity as a function of the harmonic order for epoxypropane (a) and fenchone (b), where red and blue traces correspond to *S*- and *R*-enantiomers, respectively. The gray line represents the non-chiral reference. Reprinted from [72] with permission. Copyright © 2015, Rights Managed by Nature Publishing Group.

cross-channels (recombination with a different state). Cross-channels involve magnetic dipole transitions and are inherently enantioselective. The measurement performed in epoxypropane indicates the presence of a destructive interference leading to strong suppression of the signal coming from the direct channels at harmonic 41, with a corresponding enhancement of the chiral signal coming from the cross-channels. On the other hand, in fenchone (a large polyatomic molecule) lots of cationic states are involved and large dipoles lead to substantial population transfer between the electronic states. As a result, the signal from chiral-sensitive cross-channels is comparable to that from the direct channels and destructive interference between specific channels is not needed to reveal the chiral signal. This enantiomer-sensitive method of chiral HHG could open new and important perspectives in understanding the role of the electronic dynamics in the light-induced chiral response, which is of fundamental importance in a number of chemical and biological processes.

As mentioned above, HHS has been proposed as an alternative technique to attosecond photoelectron/ion spectroscopy for tracking in real time the ultrafast hole dynamics induced by sudden ionization of molecules. Compared to the method described in section 3.2, HHS intrinsically provides higher time resolution, as the electron recollision process is used as a probe for the charge dynamics.

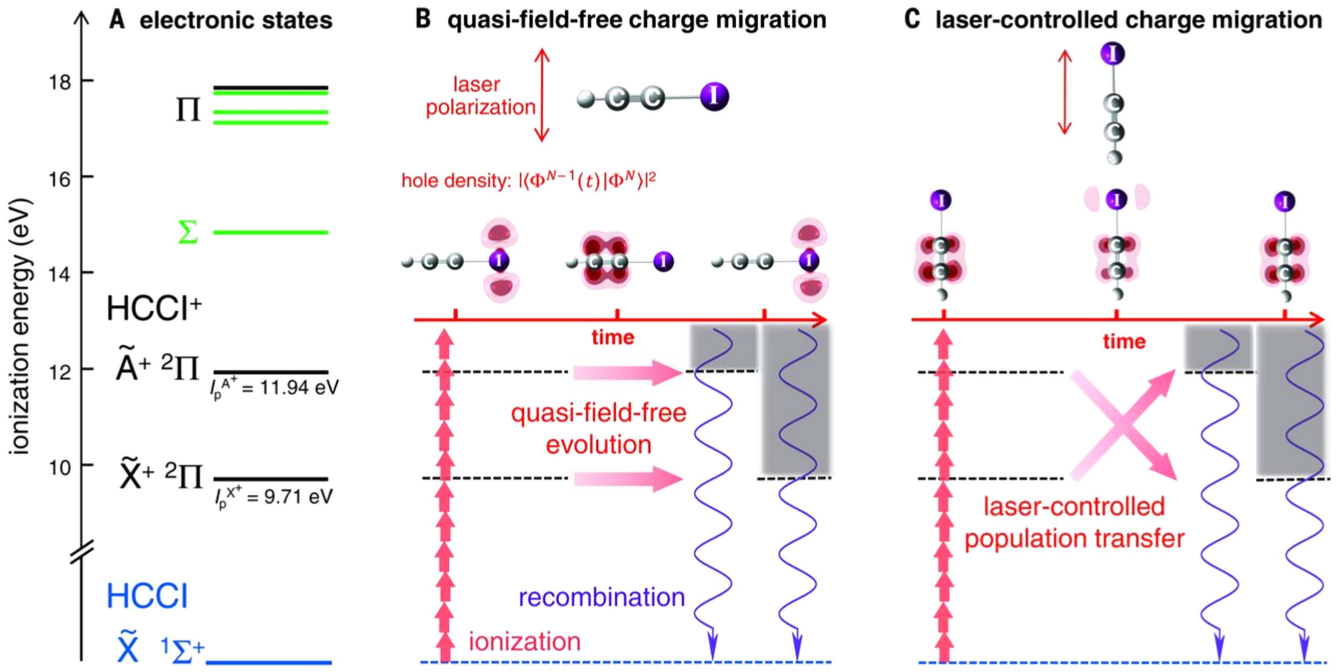


Figure 10. (a) Electronic states of $HCCI^+$. (b) Quasi-field-free charge migration and (c) laser controlled charge migration induced in iodoacetylene molecule, when the molecule is aligned perpendicular (b) and parallel (c) with respect to the laser polarization axis. Reprinted from [51] with permission. Copyright 2015, American Association for the Advancement of Science.

On the other hand, charge migration along the molecular backbone can only be evidenced in the harmonic spectrum for aligned and oriented molecules, thus limiting the number of molecular species which can be investigated. The first experiment based on HHS capable of capturing sub-fs charge migration in a polyatomic linear molecule (iodoacetylene) has been recently reported by Kraus *et al* [51]. In this experiment, the control over the spatial orientation of the molecule was exploited to separately reconstruct *quasi-field-free charge migration* and *laser-driven charge migration*. The measurement of both amplitudes and phases of high-harmonic emission from the oriented ensemble at multiple driving wavelengths (800 and 1300 nm) allowed two different mechanisms occurring in the iodoacetylene cation after strong field ionization to be distinguished. Figure 10 shows a schematic of the different charge migration precesses initiated in the molecule: in the case of laser polarization perpendicular to the molecular axis (panel (b)), strong-field ionization by infrared photons (red arrows) prepares a superposition of two electronic states ($\tilde{X}^+$ and $\tilde{A}^+$) whose evolution is encoded in the high-harmonic emission (violet arrows) at the instant of recombination. Since the superposition of two electronic states creates a charge beating with a periodicity which corresponds to the energy separation between the two states (1.85 fs), in this case a quasi-field-free charge migration between the iodine and acetylene side of the molecule was observed. On the other hand, a laser field polarized parallel to the molecular axis induces a strong population transfer between the two electronic states (panel (c)) and charge migration can be controlled by changing the driving field wavelength (laser-driven charge migration). These important results suggest that laser control could be further refined in the future to steer the hole migration to a particular site of the molecule to induce a desired chemical reaction.

4. Techniques for the production of biomolecules in the gas phase

The study of complex molecules isolated in the gas phase, particularly those of biological interest, is highly desirable even if this is not the environment in which they are normally found. In vacuo, the whole molecule, or sub-structures thereof, can be studied free from the influence of the environment allowing its intrinsic properties to be deduced via a bottom-up approach. This also is a convenient template for comparison with theoretical models which are more tractable if the molecule can be treated on its own. From a more practical point of view, if XUV light (with a penetration depth of around 100 nm in water) is used as a pump or probe and the outcome is interrogated via ion or electron spectroscopy, then the molecules must be in the gas phase or at a vacuum interface.

4.1. Vaporization/desorption methods

Generating useable gas phase densities of large labile molecules is not straightforward as sublimation rates are often too low at temperatures below which thermal decomposition occurs. Simple heating of a sample is sufficient for smaller stable molecules like some amino acids and DNA bases, particularly if the time for which the molecules possess high internal temperatures is limited. For example molecules can be produced from a heated oven and then entrained into a

supersonic gas expansion to form a molecular beam (see [73] for a recent example).

The jet is formed by expansion of a high pressure rare gas into vacuum via a pulsed valve to produce an internally cold gas. Sample molecules are dragged into the flow via collisions with the gas, reducing their vibrational and rotational energies in the process. It is more difficult to pick-up and cool larger molecules as they have a greater internal energy and lower cooling rate so that a heavier carrier gas such as Xe may be required [74]. More efficient pick-up occurs if the molecules are evaporated into a channel coupled to the nozzle exit than for an open arrangement [75, 76]. This increases the production of clusters which may not be desirable, particularly if only the isolated molecules are being studied.

In the last 30 years alternatives to simple heating for liberating molecules in the gas phase have been developed which have enabled a range of species to be produced in ionic or neutral form. The most striking advances have been the development of electrospray ionization (ESI) and matrix-assisted laser desorption and ionization (MALDI) from which macromolecules like proteins can be produced as protonated or de-protonated ions. Since these are readily coupled to mass analyzers, this has revolutionized mass spectrometry of biological species, for which Tanaka [77] and Fenn [78] were awarded the Nobel Prize for Chemistry in 2002.

In ESI a strong electric field is applied between the tip of a capillary containing a solution of the biomolecule and an extraction electrode. This field produces a spray of highly charged droplets containing the solvent and sample. The droplets shrink in size through Coulomb explosion and solvent evaporation until only isolated ions remain. The main advantage of ESI is that it is a very soft ionization method but the ion densities are generally too low for studies of ultrafast molecular dynamics. However, a few groups have recently used ESI to trap and cool biomolecules ions to produce sufficiently high number densities for pump-probe measurements (see for example [79–82]).

When the photon sources are weaker or it is desirable to study the behavior of a molecule without the influence of mobile protons, then dense plumes of neutral species are required. A recent alternative to oven based evaporation sources is aerosol thermodesorption. Initially the molecule is embedded in a nanosized aerosol particle (typically water) produced by ejection of a solution from an atomizer mixed with a carrier gas. Colliding this nanoparticle beam with a thermodesorber heated to 100 °C or more produces a plume of intact molecules in the interaction region [83]. Alternatively, a laser can be used to evaporate the solvent from the droplets [84] or even from liquid jets [85].

The dominant technique for producing dense neutral targets of labile molecules uses some form of laser desorption. The first experiments on laser desorption were conducted in the mid-1960s [86, 87], which progressed to the point where large biomolecules (up to 10^5 u) could be produced by end of the 1980s [88]. Laser desorption is effective since the wavelength can be tuned to be preferentially absorbed by a substrate or matrix to which the sample is adsorbed or mixed. By using nanosecond laser pulses, extremely high heating rates of up to 10^{12} K s^{-1} can be achieved giving brief transient temperature rises of a few thousand K.

Although the energy barriers for molecular decomposition/dissociation might be lower than those associated with desorption, the desorption rate can still be higher. Due to the transient temperature increase and the immobility of the molecule, fewer reaction coordinates for dissociation can be accessed compared to those for desorption. Therefore the pre-exponential frequency factor in the Arrhenius rate equation is much higher for desorption than dissociation as it is entropically more favorable [89, 90]

$$k_{\mathrm{des}} = [\theta]_{\mathrm{ads}}\, \nu_{\mathrm{des}} \exp\left(-\frac{E_{\mathrm{des}}}{kT}\right),$$

$$k_{\mathrm{diss}} = [\theta]_{\mathrm{ads}}\, \nu_{\mathrm{diss}} \exp\left(-\frac{E_{\mathrm{diss}}}{kT}\right),$$

where $[\theta]_{\mathrm{ads}}$ is the number of adsorbed molecules, ν is the frequency factor, E is the energy barrier to reaction, and T is the temperature of the surface. For temperatures at which k_{des} is sufficiently high for experiments, $k_{\mathrm{des}}/k_{\mathrm{diss}}$ can still be much greater than 1 even if $E_{\mathrm{des}} > E_{\mathrm{diss}}$, as long as $\nu_{\mathrm{des}} \gg \nu_{\mathrm{diss}}$. Therefore laser desorption has been successfully employed to generate a wide range of molecules in the gas phase for a variety of absorbing co-materials either used as a substrate or matrix. Graphite is a commonly used substrate as it absorbs strongly at all wavelengths and is a good heat conductor. Other substrates used include metals, porous silicon [91], or nanopatterned surfaces [92]. Although the molecule may not directly absorb the light, the ablation of material from the surface necessarily results in contamination of the plume which can preclude photoelectron spectroscopy experiments. It is also necessary to immediately cool the hot molecules in a gas jet. To ensure efficient of pickup by the jet and reduce the interval between desorption and cooling, the sample is placed as close to the exit of a pulsed valve without disrupting the flow characteristics. After skimming of the beam, the efficiency with which material is transported to the interaction region is only of the order of 10^{-6}, but given that large amounts can be desorbed per laser shot this technique has been developed by a number of groups [93–99].

More efficient transfer of laser energy into the desorption process can be obtained with the use of a matrix. Graphite powder and the biomolecule under study can be mixed in a 1:1 ratio and hydraulically pressed into a pellet which is used as the target. This increases the available sample improving the longevity and the shot-to-shot reproducibility [75, 76]. For MALDI the matrix typically has a UV chromophore which absorbs at the wavelength of a N_2 (337 nm) or Nd:YAG (3rd harmonic, 355 nm) laser. The sample and matrix are dissolved in a solvent and then co-crystalized on a substrate. The process by which the sample is ablated from the surface and subsequently charged remains a topic of debate [100, 101]. While MALDI is primarily used to generate ions for mass spectrometers, the proportion of ions to neutrals is low (less than 10^{-4} [102]) meaning there is a substantial density of neutrals which could potentially be used as a molecular target [103].

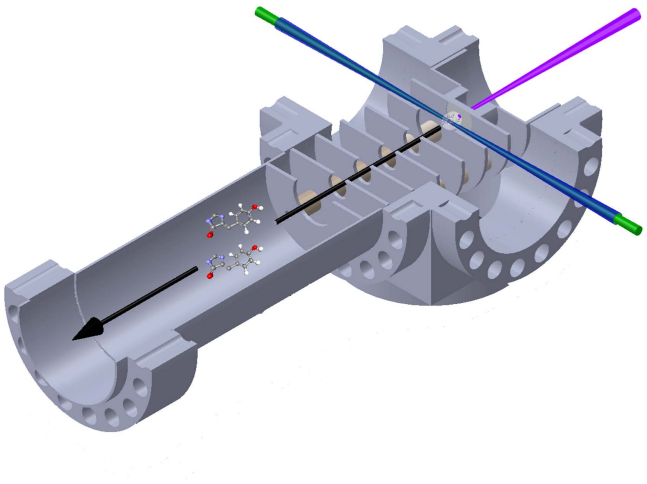


Figure 11. Schematic of the experimental set-up used for LIAD and LITD.

Direct laser irradiation of the sample is unsuitable for experiments where a pure molecular target is needed. Cleaner plumes and gentler desorption can be produced by employing LIAD since the sample is not directly irradiated with this technique. The sample is dried or pressed onto a metal foil with a thickness of around 10 μm and the opposite side of this foil is irradiated with a nanosecond laser to liberate a plume of molecules from the foil. While this technique was first demonstrated in 1985 [104], its adoption has been slow due to the need in most cases for post-ionization to detect the molecules [105, 106], but more recently there has been a revival of interest (see for example [63, 107–112]). There remains a lack of understanding of the desorption mechanism, although the intense acoustic wave generated by the rapid expansion of the irradiated foil is believed to be responsible. However, the velocity of the foil surface is much lower than that needed to initiate a direct shake-off mechanism [109]. Desorption from the surface also occurs well after the acoustic wave has dissipated and it is not clear how the acoustic frequencies (up to 10^{11} Hz) can disrupt adsorption bonds with much higher frequencies (10^{12}–10^{13} Hz).

Heating of the foil by the laser, both during each laser pulse and from the average over multiple pulses cannot be ruled out. This seems to be supported by observations that the liberated molecules are quite hot [63] and for the most part only desorption of relatively stable molecules has appeared in the literature. Zinovev *et al* [113] conclude that LIAD is actually a misnomer and desorption is most likely due to the thermal and mechanical stresses between the sample and foil.

Typical intensities used for desorption are between 10^{8}–10^{9} W cm^2, but recent tests by the current authors have shown that the energy deposited per unit area appears to a more critical parameter. Using pulses of 100 ps duration with energies a factor of 10 lower than typical, but with intensities up to 10^{11} W cm^2, did not produce any desorption. Surprisingly a CW laser has proved capable of producing molecular targets for a range of samples such as amino acids, the green fluorescent protein chromophore, and DNA nucleosides [49, 50, 114–116]. A schematic of the experimental set-up is shown in figure 11.

Since use of a CW can only produce heating, this process is more accurately described as laser induced thermal desorption (LITD). The molecules produced by LITD appear less susceptible to decomposition than molecules produced from an oven. This may be due to the fact there is a short time between evaporation from the surface and transport to the interaction region, whereas in an oven the molecules may go through several cycles of evaporation and condensation before being liberated.

To date neither LIAD nor LITD have been coupled to a gas jet immediately after desorption. Irrespective of the exact desorption mechanism, this would enable the excess energy in the molecules to be removed which would substantially improve their stability. This could allow much larger species to be produced without the contamination of substrate or matrix material which is unavoidable for direct laser desorption.

4.2. Molecular conformer selection

While cooling in a gas jet allows intact molecules to be transported to the interaction region with low internal energy, there will be a distribution of structural isomers due to rapid cooling into local minima in the potential energy landscape. As described in the next section, these structural variations can result in substantial change in the molecular dynamics so that observations are an incoherent average of the conformational distribution. Therefore, if charge migration experiments are to be fully investigated in the future and compared with the most accurate theoretical models, then techniques for selecting specific conformers of complex molecules will need to be applied.

While conformers are challenging to distinguish, small differences in their physical properties can be exploited to select specific conformers from an ensemble. For instance, geometrical changes give different collisional cross sections which can be used in ion mobility spectrometry to separate conformers in a drift tube. In principle current techniques which combine ESI and ion traps could be augmented with an ion mobility spectrometer to create conformationally selected bunches of ionic molecules. These methods have already been used to study photoisomerization reactions [117], but creating sufficient densities for pump-probe studies would be very challenging.

Alternatively spectroscopic differences in the vibrational spectrum could be exploited. These arise from changes in the position and strength of intramolecular H-bonding which alters the vibrational structure within electronic absorption bands of chromophores. For instance the absorption peaks in the spectra of aromatic amino acid conformers differ by around 1–10 meV [118–120]. Therefore, a tuneable ultraviolet laser pulse with a duration of a few picoseconds could be used to selectively excite a specific conformer. An ultrashort pump pulse with photon energy below the ionization energy would then be able to ionize this excited state to

launch an electronic wavepacket in the cation of a distinct conformer.

The technique which is currently at the most advanced stage of development is separation of conformers with different permanent electric dipole moments. If a molecular beam is passed through an inhomogeneous electric field ϵ, the force on each conformer $\underline{F} = \mu(\epsilon).\ \underline{\nabla}\epsilon$ is proportional to the effective dipole moment $\mu(\epsilon)$ which is determined by the particular quantum state populated for each conformer. To populate only the lowest rotational states of the molecule and reduce the transverse momentum, cooling down to 1 K is necessary. Using an AC electric field produced in a multipole electrode arrangement, the molecular beam can be focussed strongly so that only the conformer with the weakest dipole moment is transmitted [121, 122]. Alternatively, using an inhomogeneous DC field to deflect the beam, conformers can be spatially separated. With this arrangement, separation of the *cis* and *trans* isomers of aminophenol and fluorophenol has been achieved where the dipole moments differ by more than one Debye [123, 124]. For more complex molecules of interest for charge migration experiments, a greater number of conformers will make selection more difficult. For example, in phenylalanine at least six conformers are likely to have significant populations in a molecular beam. Three of these have dipole moments around 1.5 D with the others close to 6 D [125]. So while narrowing of the conformational distribution is currently possible, individual conformer selection will remain a challenging task for some years to come.

5. Theoretical models for the description of electron dynamics in bio-relevant molecules

The rapid developments in attosecond technology has resulted in an increasing number of gas-phase experiments on atoms [126–129] and hydrogen molecules [11, 130, 131], where attosecond control of electron dynamics has been attained. The interaction of these targets with ultrashort pulses has been relatively well understood by means of *ab initio* methods whose accuracy allows the prediction of unforeseen phenomena and the design of novel experimental applications such as those based on XUV-pump/XUV-probe schemes [19, 132]. A time-resolved picture of molecular electron dynamics in biologically relevant molecules, or equivalently, obtaining a reliable representation of electronic wave packets evolving in these systems on the few-femtosecond or sub-femtosecond time scales, is the first step to understand relaxation and fragmentation dynamics, and therefore to achieve attosecond control of biologically relevant processes [133]. However, a theoretical description of the correlated motion of electrons and nuclei that follows ionization by attosecond pulses is still challenging even for the H_2 molecule [134, 135], and out of reach for many-electron polyatomic molecules. Among the most promising approaches, we could mention recent extensions of the multi-configurational time-dependent Hartree–Fock method [136–141]. The most recent progress towards its implementation have enabled the description of photoionionization events incorporating the nuclear degrees of freedom beyond the Born–Oppenheimer approximation, although it is only computationally affordable in the treatment of diatomic molecules [142–144]. Even in the framework of frozen nuclei, reliable theoretical tools for the description of electron dynamics in large molecules such amino acids are still scarce.

The investigation of ultrafast phenomena triggered after ionizing gas-phase biomolecules faces a number of major challenges [6, 132, 145]: (i) description of the electronic structure (potential energy surfaces, electronic dipole elements, etc, of an N-electron system) for both the neutral and resulting molecular ion, (ii) a realistic representation of the electronic wave packet upon photoionization, in other words, accurate evaluation of the ionization amplitudes, (iii) identification of the observables that are relevant for a given experimental measurement and (iv) inclusion of nuclear degrees of freedom and the coupling with the electronic motion. Besides these critical points, there are countless issues that remain open, as for instance, the effect of the ejected electron in the observed dynamics. One would expect it to be only important at short times, say for a few hundreds of attoseconds, which is the estimated time that one electron would take to escape from the molecular potential and effectively leave a $(N-1)$-electron target behind. However, more sophisticated approaches are required to definitively disregard, for instance, many-body effects which are already known to induce decoherence in the hole wave packet in specific cases as shown in atomic photoionization [146].

To face challenge (i), i.e., the description of electronic structure of large molecules, one can make use of a large variety of existing quantum chemistry packages, which provide accurate electronic energies and structural information [147–156]. Restricted to the description of bound states, they can provide, e.g., accurate transition dipole moments for radiation-induced excitation processes, magnetic properties, or analytical gradients and non-adiabatic couplings to explore molecular relaxation phenomena. Among the available tools employed in recent works to explore laser-induced processes in biomolecules are those based on density function theory (DFT) [148–150, 154] and the post-Hartree–Fock methods [147, 150, 152–155]. On the one hand, DFT methods make use of the electronic density to reformulate the N-electron problem into a one-electron problem, leading to a good compromise between accuracy and computational effort. Standard DFT methods go beyond the Hartree–Fock approach because they include electron correlation, still by means of a single Slater determinant, through exchange-correlation functionals that have been shown to provide accurate descriptions for the electronic ground states of many-electron systems. In practice, because of the use of a single Salter determinant, DFT methods are usually limited to the description of singly excited electron states. On the other hand, the so-called post-Hartree–Fock methods are based on configuration interaction approaches, in which the wave function is represented as a combination of several Slater determinants explicitly including electron correlation, which is mandatory to describe phenomena where more than one active electron is involved (double excitations, Auger decay

processes following inner-shell ionization) [157] or processes involving relaxation pathways through states with a multi-reference character, such that conical intersections. It is worth stressing that, despite their complexity, these academic or commercial quantum packages, either based on DFT or post-Hartree–Fock methods, are restricted to the description of bound or excited molecular states. Additional work is thus necessary to obtain, for instance, core-hole states or electronic continuum states to compute reliable photoionization amplitudes for large molecules. In spite of these limitations, in particular, the impossibility to describe ionization, theoretical calculations performed more than fifteen years ago by Cederbaum and co-workers were already able to predict and describe charge migration phenomena in ionized biomolecules by using artificially prepared initial electronic wave packets [1, 2]. Their results showed that charge migration occurs in a few femtoseconds, a result that has been confirmed experimentally a few years later [48, 49]. The short time required by the charge to migrate from one side of the molecule to the other, suggested that nuclear motion, not included in those simulations, could indeed be ignored. By using the same methodology, charge migration has been investigated over the years, from small amino acids such as glycine [158, 159] to larger molecules containing aromatic rings [59]. In these works, time propagation of the electronic wave packet was performed by using a Green's function method, the so called non-Dyson ADC(3) (algebraic diagrammatic construction) approach [4]. In 2006, Remacle and Levine used DFT to estimate charge migration times within a tetrapeptide (1.5 fs) [3], in reasonable agreement with the previous findings. Again, there was no explicit evaluation of the continuum states and the dynamics in the cation was treated as in the previous works.

The calculations described above demonstrated that electron correlation can drive pure electron dynamics in the sub-femtosecond time scale. However, as we will see below, ionization by attosecond pulses can also lead to electron wave packets that evolve in a similar time scale without the need for electron correlation. For this, an accurate description of the ionization step is required (challenge (ii) mentioned above). Since this is a crucial aspect to fully understand electron dynamics induced by attosecond pulses, we will devote a few lines to describe in some detail how ionization was accounted for in those early approaches. In those works, ionization was described by just removing an electron from a specific molecular orbital of the neutral biomolecule (sudden ionization). In other words, the electronic state describing the molecular cation was built by creating a Koopmans hole (a hole in a ground state Hartree–Fock orbital). In this approach, the ionization process is assumed to be very fast, so that that the remaining electrons are still described by the unrelaxed HF orbitals, i.e., ionization is completed before relaxation and correlation takes place in the cation. Therefore, the resulting hole state is not a stationary state of the cation, but a linear combination of cationic eigenstates, which then evolves with time. The hole generated in this way moves across the molecular chain inducing a site-selective reactivity related to charge localization in a particular site of the molecule. When ionization is induced by attosecond pulses, which are associated with broad-band distributions covering a few tens of eV, the induced dynamics is very different, since electrons are removed from several molecular orbitals of the neutral molecule, not just one. As in the previous case, one creates a non-stationary state of the parent ion that will evolve in time, however, at variance with that case, a realistic description of the coherent superposition of cationic states created by the attosecond pulse requires the accurate evaluation of the ionization amplitudes, i.e., of the molecular continuum states. Efforts towards extending available quantum chemistry packages to describe ionization are currently under development [49, 50, 57, 133, 160]. These approaches seek to solve the actual scattering problem associated with having electrons in the continuum, although in their current form, such continuum electrons are simply described by Coulomb functions. These are the exact continuum wave functions of the hydrogen atom and, therefore, they do not describe the multi center character of the molecular potential nor the effect of the remaining electrons. Nevertheless, in spite of its simplicity, this is a significant step forward compared to methods based on the Dyson norm [161, 162], which results from projecting the initial state of the neutral molecule onto the final cationic states (in some way, the early methods described in [1, 3] belong to this category). Indeed, although a very small Dyson norm is almost always associated to a very small ionization probability, the opposite is not necessarily true, since large Dyson norms can be associated with small transition dipole matrix elements. More sophisticated approaches that go beyond the use of Coulomb functions, solve the scattering equations by assuming a HF-like description of the system [163, 164] of make use of the Kohn variational principle [165–167], however they are only feasible for diatomics or small polyatomics.

The first theoretical calculation of an actual electronic wave packet resulting from ionization of a large molecule with an attosecond pulse was reported in 2014 for the case of the phenylalanine molecule [49]. The wave packet was built from ionization amplitudes resulting from the solution of the actual scattering equations in the framework of the static exchange DFT method developed by Decleva and collaborators [168]. As previously discussed, single-active electron methods as DFT are reasonable for valence-shell ionization, as long as shake-up/shake-off processes are not important, i.e. provided that excitation-ionization processes, where one electron is ejected while a second electron is promoted into an excited state, play a minor role. This is the case when electrons are mainly ionized from the outer valence shells, as in the work reported in [49]. The static exchange DFT methodology had already been shown to provide accurate photoionization cross sections for both small and large molecules irradiated with synchrotron radiation [169–173]. Recent extensions of this method include the computation of a time-dependent electron density, which was achieved through the implementation of first-order time-dependent perturbation theory expressions [49, 50]. More details will be given below.

The third important issue mentioned above (challenge (iii)) is to identify the relevant observables. The time

evolution of the electron density in the parent ion is the property that is evaluated in most theoretical works reported above. However, it is not obvious to relate this property with observables measured in real experiments: electron and ion yields, absorption spectra, mass spectra, electron and ion angular distributions, etc. In this respect, there has been already an attempt to go beyond analyzes based on the electron density and to provide molecular-frame photoelectron angular distributions that can be directly compared with the measured ones [174]. However, the comparison suffers from limitations in the description of the electronic continuum, which is represented by orthogonalized plane waves.

Finally, inclusion of the nuclear dynamics and its coupling to electron dynamics (challenge (iv) above) may have a significant effect, since it can induce decoherence in the charge migration process [132]. As it has been explained, most works have assumed that prompt ionization by an attosecond pulse leads to charge migration preceding any nuclear rearrangement and have explored the problem within the fixed-nuclei approximation. In this framework, results were expected to be reliable in an interval covering the first tens of femtoseconds [1–3, 49, 174–176]. Only very recently, a few theoretical works have been able to account for the nuclear motion at different levels of approximation [51, 57, 177–179]. For instance, Robb and collaborators [178] have implemented a semiclassical approach, by using the Ehrenfest method in combination with a CASSCF formalism, to show that nuclear motion may have a more important effect than previously anticipated. In particular, they have studied the variation of the dipole moment in glycine and Gly-Gly-NH-CH3 generated by an ad hoc coherent superposition of two electronic states around a conical intersection. Their results show that coherence of such electronic wave packet only survives for a few femtoseconds. Attosecond charge migration has also been observed from high-harmonic generation experiments on iodoacetylene [51]. Theoretical modeling of this experiments has included the effect of the nuclear motion through the so called nuclear autocorrelation function, which is given by the Franck–Condon overlap between the ground vibrational state of the neutral molecule and the time-evolved NVP in the cation. In [57, 177], nuclear motion is included by performing an average, over all normal modes, of several hole propagations at different fixed-nuclei geometries. They found that electron dynamics triggered in the benzene cation [177] survives more than 10 fs, confirming that hole migration is still visible in the presence of nuclear motion. In [57] the outcome is however quite distinct, since they found that the interaction of PAHs with XUV pulses launches an electron dynamics involving excited cationic states that undergo a fast relaxation, shorter than the typical vibrational periods, due to non-adiabatic couplings through conical intersections. Nuclear motion can thus play a critical role in some specific cases, depending on the states involved (inner or valence-hole states, doubly excited states, etc) and how they are accessed upon excitation or ionization with light. In particular, calculations reported to explore charge migration in phenylalanine [49, 50] were carried out within the fixed-nuclei approximation and they are in very good agreement with the experimental data. The shortest estimated vibrational period in this molecule is around three times larger than the period of the measured electronic fluctuations, in agreement with the above-mentioned findings for glycine or benzene. Finally, it is worth mentioning that there is work in progress to include nuclear motion in a fully quantum mechanical manner. This has been already done in the framework of the static exchange DFT method within the Born–Oppenheimer approximation for diatomics [180–183] as well as for small polyatomics in processes where the nuclear degrees of freedom can be reduced to a single mode (usually the symmetric stretching) [184–186]. However, near-future attempts to include nuclear motion in biomolecules will be likely restricted to semiclassical approaches.

5.1. Static-exchange DFT formalism

The static exchange DFT approach was developed by Decleva and collaborators over the last decade. The original method, designed to work within the fixed-nuclei approximation, is given in detail in [168–170, 187, 188]. For this reason, only the essentials are reviewed here. In brief, the key idea is to use the Kohn–Sham DFT formalism to describe the ground state and to obtain the corresponding Kohn–Sham density of the neutral molecule. The latter is then used as the electron interaction term in a new hamiltonian that will be diagonalized by writing the continuum electron wave function in a numerical basis and imposing the proper boundary conditions of the multichannel scattering problem that defines molecular photoionization.

Firstly, a standard DFT calculation is performed to obtain the ground state of the neutral molecule, using the LB94 or the LDA functional to include exchange and correlation effects [189]. The Kohn–Sham orbitals for the ground state and the electron density are expressed in terms of Slater type orbitals (STOs) and are later rewritten as a function of B-spline basis functions. In the traditional linear combination of atomic orbitals expansions, STOs or Gaussian type orbitals are employed. Their suitability to describe bound states comes from the fast convergence by using relatively reduced basis sets. However, linear dependencies are well-known to appear for the computation of unbound states and even for bound excited states if there is a large overlap between expansions in different centers. The use of piecewise polynomials, such as B-spline functions, solves these problems and allows for a good description of electrons in the continuum, at the cost of a slower convergence for the bound states.

For illustrative purposes, the Kohn–Sham orbitals computed for the amino acid phenylalanine are plotted in figure 12. The figure only shows the orbitals that are accessible by the experimental attosecond pulses described in previous sections. The orbitals correspond to the most stable conformer at the experimental temperature in [49, 50], after geometry optimization at the DFT/B3LYP [190, 191] level with a 6-311+g(3df, 2p) basis set and using as initial guess the optimized geometries reported in [125, 192, 193] (calculations were performed by using the quantum chemistry package Gaussian09 [155]). The orbitals were then computed

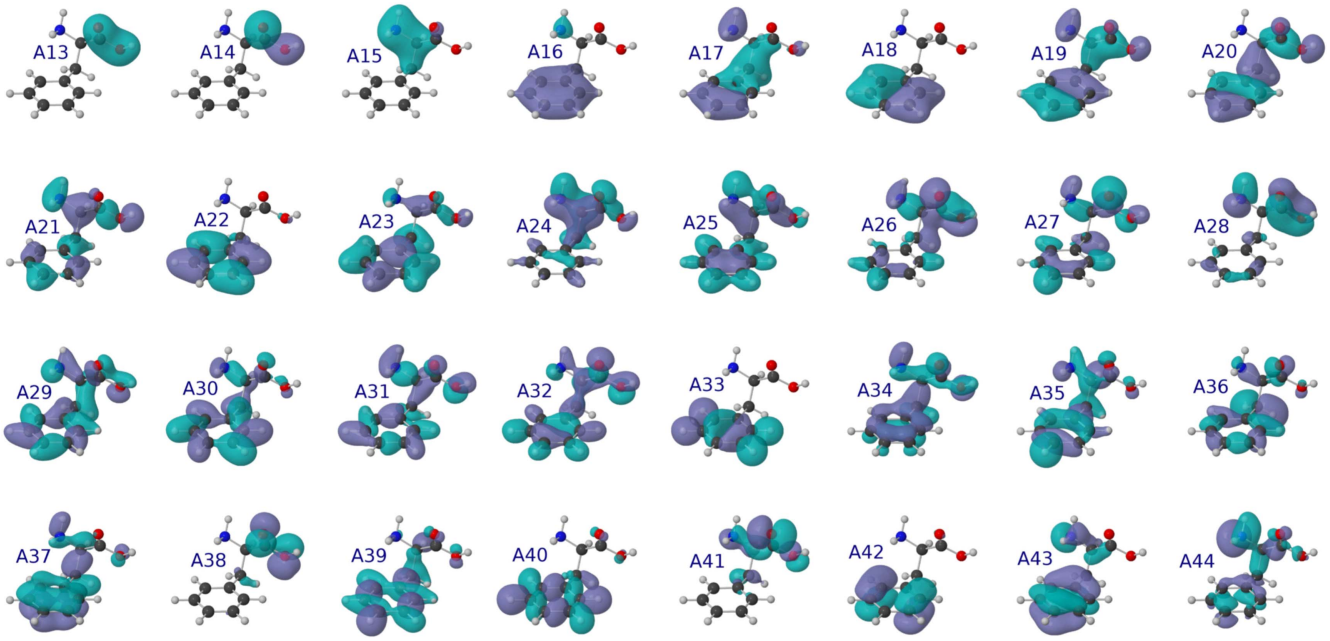


Figure 12. Occupied Kohn–Sham orbitals of the phenylalanine molecules obtained using the LB94 functional in a basis set of B-spline functions as explained in the text.

with the Amsterdam density functional package [148, 194] using the LB94 functional.

The continuum states are then built by promoting one electron from a bound spin orbital ϕ_α to a continuum orbital $\phi_{\varepsilon lm}$ with kinetic energy ε and angular quantum numbers l and m,

$$\Psi_{\alpha\varepsilon lm}(\mathbf{x}_1, \mathbf{x}_2, \ldots, \mathbf{x}_n) = |\phi_1\phi_2 \ldots \phi_{\alpha-1}\phi_{\varepsilon lm}\phi_{\alpha+1} \ldots \phi_N|. \quad (1)$$

Bound and continuum orbitals are evaluated using symmetry-adapted products of B-spline functions for the radial components and spherical harmonics for the angular part. To improve convergence, a multi-centric basis set of B-splines is defined, with symmetry-adapted linear combinations of real spherical harmonics with origin over different positions in the molecule: (i) A large one-center expansion (OCE) over the center of mass of the molecule provides an accurate description of the long-range behavior of the continuum states. (ii) Small expansions, called off-centers (OCs), located over the non-equivalent nuclei, complement the OCE. The OC sets efficiently describe the Kato cusps at the nuclear positions, giving an accurate description of the bound states even for relatively low angular expansions in the OCE. The basis set elements may be written in the multi-centric basis as

$$\xi^p_{nlh\lambda\mu} = \sum_{q\in\Lambda_p} \frac{1}{r_q} B^\kappa_n(r_q) \underbrace{\sum_m b^q_{mlh\lambda\mu} Y_{lm}(\theta_q, \varphi_q)}_{X^p_{lh\lambda\mu}(\theta_q,\varphi_q)}, \quad (2)$$

where Λ_p represents a shell of equivalent centers ($p = 0$ refers to the OCE), q runs over the centers in the shell, n is the index that runs over the B-spline functions B^κ_n, $\lambda\mu$ are the indexes of the irreducible representation (see [168]), h runs over the angular functions constructed as linear combinations of real spherical harmonics associated to a fixed angular quantum number l, and the coefficients $b^q_{mlh\lambda\mu}$ are determined by symmetry defining the so called symmetry-adapted spherical harmonics $X^p_{lh\lambda\mu}$, which transform acording to the irreducible representations under the symmetry operations of a given point group. In each center q, the B-spline expansion reaches a maximum value $R^p_{\max}$, which can be different for non-equivalent centers. A large vale of $R^0_{\max}$ is required in the OCE in order to provide a good description of the oscillatory behavior of the continuum states. One can control the overlap between the basis elements, avoiding running into linear dependences, by keeping small OC expansions ($R^{p>0}_{\max} \simeq 1$ a.u.) since the Kato cusps are usually well localized at the atomic positions. Angular expansions are truncated so l takes values up to a maximum $l^p_{\max}$, which can also be different for the non-equivalent centers. In general, one can keep small values of $l_{\max}$ in the OCs to complement the OCE in the description of the bound states, but a large angular expansion is usually required in the OCE, especially in the case of complex molecules and for the evaluation of continuum states with high kinetic energy.

The diagonalization of the Hamiltonian matrix generated from the DFT density leads to a complete orthogonal set including both bound and continuum orbitals. The latter are obtained through the Galerkin approach described in [196]. In this approach the continuum function does not vanish at the end of the box and it can be obtained for any specific energy E chosen *a priori* as a solution of the secular eigenvalue problem (see [170, 195, 196]), relative to the smallest eigenvalues

$$(\mathbf{H} - E\mathbf{S})\mathbf{c} = a\mathbf{c}. \quad (3)$$

The correct normalization for the continuum states, i.e. imposing the proper scattering boundary condition, is then obtained by fitting the numerical solutions to proper linear

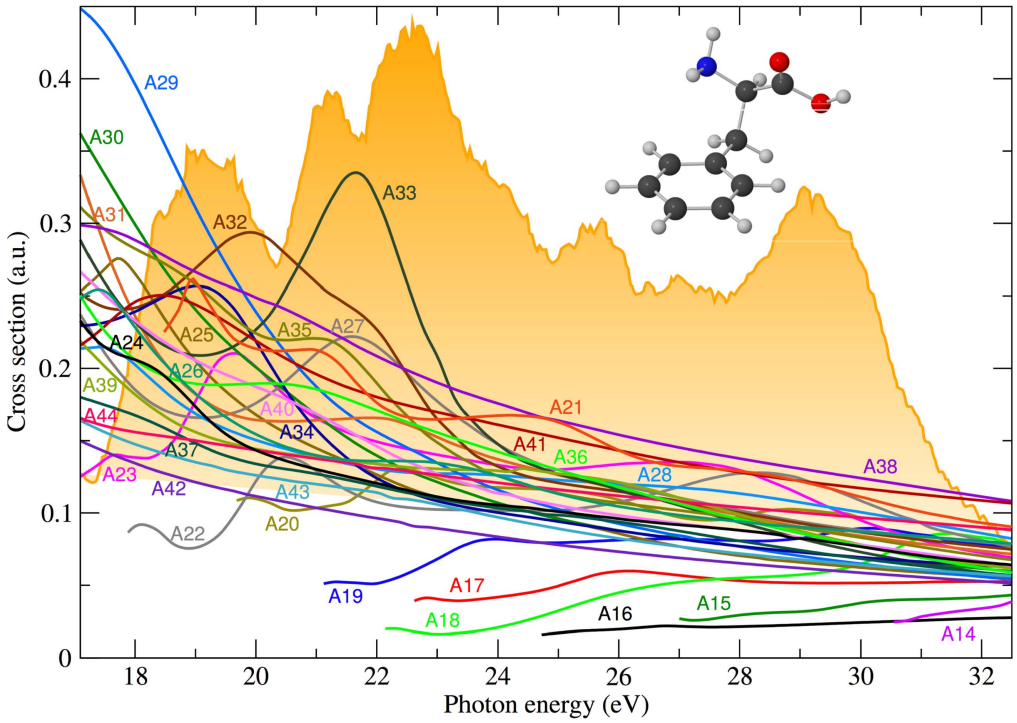


Figure 13. Photoionization cross sections of phenylalanine from different molecular orbitals calculated using the static-exchange DFT method. Numbers and colors denote the molecular orbitals from where the electron is emitted in each case. The filled orange line in the background corresponds to the energy spectrum of the attosecond pump pulse used in the experimental set-up shown in section 3.2 and plotted in figure 8.

combinations of regular and irregular asymptotic (Coulomb) functions at the outer radius.

The laser-molecule interaction is then treated within the dipole approximation and evaluated in the length gauge, $V(t) = \boldsymbol{\mu} \cdot \mathbf{E}(t) = \sum_{i=1}^{N} q_i \mathbf{r}_i \mathbf{E}(t)$, where $\boldsymbol{\mu}$ is the dipole operator and $\mathbf{E}(t)$ the electromagnetic field. In our description of the wave function, the residual ion remains frozen (static-exchange approximation), which reduces the evaluation of the dipole transition element, $\langle \Psi_{\alpha\varepsilon lm}(\bar{\mathbf{x}}) | \boldsymbol{\mu}_{\boldsymbol{\epsilon}} | \Psi_0(\bar{\mathbf{x}}) \rangle$, to the calculation of the coupling between the bound orbital where the electron is taken from ϕ_α and the continuum orbital where it is promoted, $\phi_{\varepsilon lm}$, with $\boldsymbol{\epsilon}$ being the polarization direction of the field. The total photoionization cross sections are simply defined, within the first-order perturbation theory, as proportional to the square of the dipole transition element:

$$\sigma_{\epsilon\alpha}(\varepsilon) = \frac{4\pi^2\omega}{\hbar c} \sum_{lh} |\langle \Psi_{\alpha\varepsilon lh}(\mathbf{x}) | \boldsymbol{\epsilon} \cdot \boldsymbol{\mu}_{\boldsymbol{\epsilon}} | \Psi_0(\mathbf{x}) \rangle|^2. \quad (4)$$

Note that for randomly oriented molecules, one computes $\sigma_{\epsilon\alpha}$ for three orthogonal directions of the polarization vector of the field and then average the results incoherently.

The photoionization cross sections of the phenylalanine molecule obtained with this method are given in figure 13 as a function of photon energy. Numerical details are given in [49, 50]. The different cross sections, averaged over all molecular orientations, correspond to electron emission from the molecular orbitals shown in figure 12.

In figure 13, we can already see that by simply using monochromatic light, electrons can be ejected from a number of different orbitals. For instance, upon absorption of a photon of 17 eV, electrons can be ejected from the orbitals A23–A44. At 19 eV, photoionization from A21 and A22 is also open, and so on. If we irradiate the molecule with the broad energy bandwidth of an ultrashort pulse, this enables the possibility of having electrons ejected with the same energy but leaving behind different ionic states, which is the origin of the coherences observed in the electron dynamics of the cation. In the figure, the energy distribution of the experimental pulse described in section 3.2 and plotted in figure 8 is included in the background. The energetics for the neutral, the cation and the dication is depicted in figure 14. The pulse distribution is also included, as well as all the cationic states that are accessible for the energies within the pulse bandwidth.

5.2. Hole migration dynamics

One must solve the TDSE to obtain the N-electron wave function that defines the evolution of the system after the interaction with the pulsed radiation. This can be done by expanding the time dependent wave function in the basis of eigenstates of the isolated molecule of equation (3):

$$\Phi(\mathbf{r}_1, \ldots, \mathbf{r}_N, t) = c_0(t) \mathrm{e}^{-\mathrm{i}E_0 t} \Psi_0(\mathbf{r}_1, \ldots, \mathbf{r}_N), \quad (5)$$

$$+ \sum_{\alpha lm} \int c_{\alpha\varepsilon lm}(t) \mathrm{e}^{-\mathrm{i}(E_\alpha + \varepsilon)t} \Psi_{\alpha lm}(\mathbf{r}_1, \ldots, \mathbf{r}_N, \varepsilon) \mathrm{d}\varepsilon, \quad (6)$$

where $\Psi_0(\mathbf{r}_1, \ldots, \mathbf{r}_N)$ is the ground state of the molecule and $\Psi_{\alpha lm}(\mathbf{r}_1, \ldots, \mathbf{r}_N, \varepsilon)$ the electronic continuum states. The wave function depends on the ionic state α created after removing an electron from the α orbital, on the angular momentum of the ejected electron associated to the α channel, lm, and on

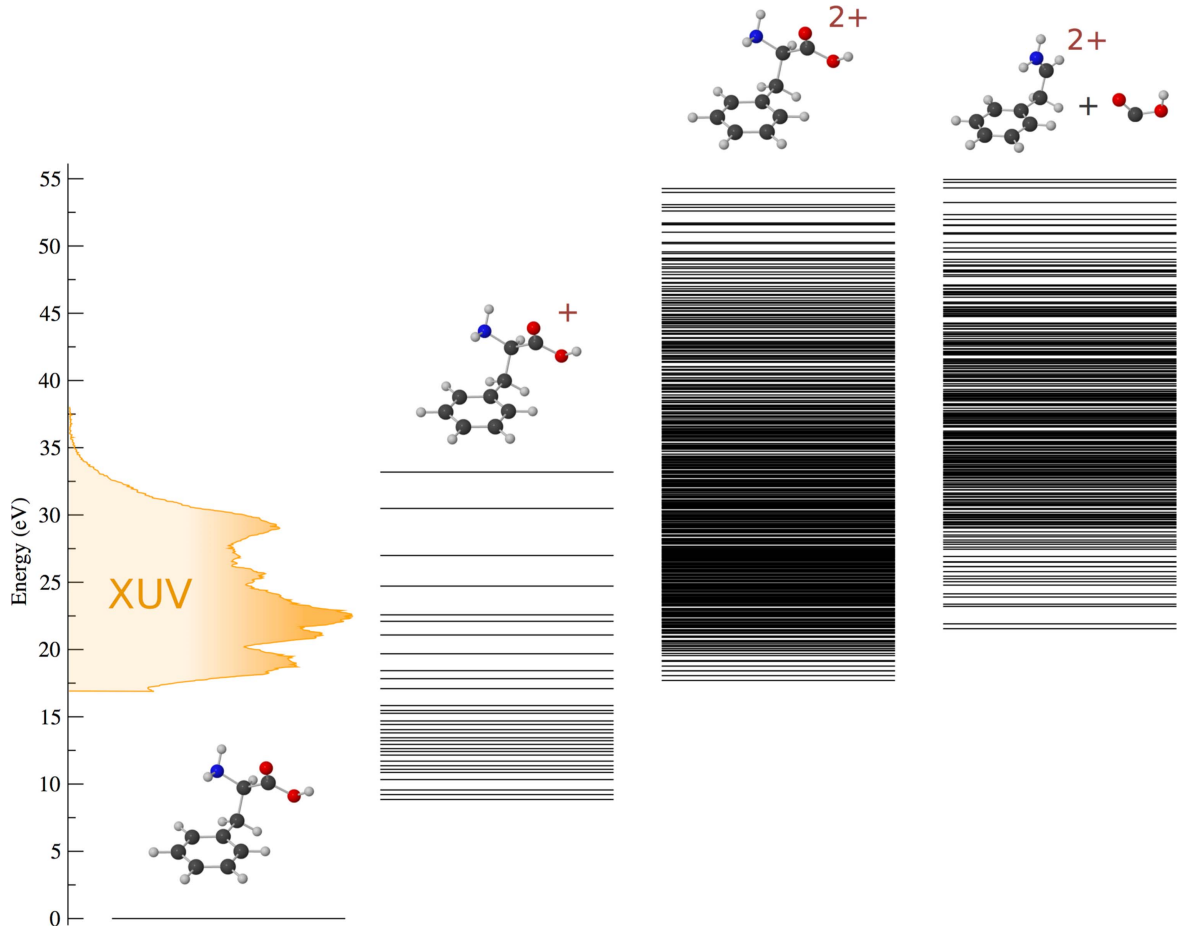


Figure 14. Energy level diagram containing all the states of singly charged phenylalanine populated by the XUV pulse, whose energy distribution is included as a shadowed area in the axis bar, all the states of doubly charged phenylalanine and those for the system doubly charged immonium + neutral carboxyl.

the electron energy, ε. For the time propagation, the continuum states are normalized to build an orthonormal basis set of eigenstates such that:

$$|c_0(t)|^2 + \sum_{\alpha lm} \int |c_{\alpha\varepsilon lm}(t)|^2 \mathrm{d}\varepsilon = 1. \tag{7}$$

The initial conditions are given by $c_0(t) = 1$ and $c_{\alpha\varepsilon lm}(t) = 0$, which represent the fact that before the interaction with the laser pulse ($t \leqslant 0$) the molecule is in its ground state. Once the action of the electromagnetic field is turned off, the expansion coefficients are given by the products of the transition amplitudes right at the end of the pulse, $c_i(t = T)$, and the stationary phases of the corresponding eigenstate, $c_i(t) = c_i(T) \cdot \exp[-\mathrm{i}E_i(t - T)]$.

Attosecond pulses used in current experiments are very weak, thus one can make use of first-order time-dependent perturbation theory to evaluate the ionization amplitudes. In this framework, they are given by the product of the dipole transition matrix element, $\langle\Psi_{\alpha lm}|\boldsymbol{\epsilon}\cdot\boldsymbol{\mu}|\Psi_0\rangle$ and the Fourier transform of the pulse:

$$c_{\alpha\varepsilon lm}(T) = -\mathrm{i}\langle\Psi_{\alpha lm}|\boldsymbol{\epsilon}\cdot\boldsymbol{\mu}|\Psi_0\rangle \int_{-\infty}^{\infty} E(t)\mathrm{e}^{\mathrm{i}(E_\alpha+\varepsilon-E_0)t}\mathrm{d}t. \tag{8}$$

The pulse can be written as

$$E(t) = \begin{cases} A(t)\sin(\phi + \omega t)\boldsymbol{\epsilon} & t \in [0, T] \\ 0 & \text{elsewhere,} \end{cases} \tag{9}$$

where $\boldsymbol{\epsilon}$ is the polarization vector, $A(t)$ is the pulse envelope, which accounts for its finite duration, T, ϕ is the carrier-envelope phase (CEP) and ω is the carrier frequency. Higher order terms are only necessary if the carrier frequency is not constant, for instance with chirped pulses. The Fourier transform of equation (9) can be then written as $\tilde{E}(\omega) = \int_0^T \mathrm{e}^{-\mathrm{i}\omega t}E(t)\mathrm{d}t$ and gives the frequency and phase distribution of the pulse. Attosecond pulses produced in the laboratory usually contain some chirp, which is often unknown. They also have a rather complicated spectral shape, which is often known. For these reasons, in order to study the dynamics triggered by attosecond pulses, it is convenient to use the experimental energy distribution $|\tilde{E}(\omega)|$, like those shown in figures 13 and 14. In the absence of more information, most calculations are performed by assuming a zero CEP and a constant phase, $\theta = \arg(\tilde{E}(\omega)) = c$, in the frequency domain.

In order to depict the charge migration phenomena triggered upon photoionization, the most extended approach is to compute the electron density of the created hole. As discussed

in previous sections, one can assume that the photoelectron is ejected very rapidly, within a few hundreds of attoseconds, and that the interaction of this photoelectron with the ion left behind is weak. Under these circumstances, one can assume that the the ejected electron and the remaining cation are completely decoupled, so that one can restrict the study of the wave packet dynamics to the $N-1$-electron system. Although this approximation implies neglecting explicitly multi-body effects upon photoionization [146], we will see below that a substantial part of the observed dynamics is the result of coherences between cationic states associated with electrons ejected with the same energy.

The time-dependent electronic density of the isolated $(N-1)$-electron ion at a given time t after the end of the pulse, $\rho_{\rm ion}^{N-1}(\mathbf{r},\,\mathbf{r}_2,...,\mathbf{r}_{N-1};\,t)$, is obtained by projecting the N-electron wave function defined in equation (5) onto the continuum orbitals $\phi_{\alpha\varepsilon lm}$ and integrating over electron energy

$$\rho_{\rm ion}^{N-1}(\mathbf{r}_1,\,\mathbf{r}_2,...,\mathbf{r}_{N-1};\,t) = \sum_{\alpha lm}\int \langle\Phi(\mathbf{r}_1,\ldots,\mathbf{r}_N,\,t)|\phi_{\alpha\varepsilon lm}(\mathbf{r}_N)\rangle_{\mathbf{r}_N}\langle\phi_{\alpha\varepsilon lm}(\mathbf{r}_N)| \times \Phi(\mathbf{r}_1,\ldots,\mathbf{r}_N,\,t)\rangle_{\mathbf{r}_N}\mathrm{d}\varepsilon, \quad (10)$$

where the brackets indicate integration over $\mathbf{r}_N$. The one-particle density matrix is defined as usual

$$\rho_{\rm ion}(\mathbf{r},\,t) = (N-1)\int \rho_{\rm ion}^{N-1}(\mathbf{r},\,\mathbf{r}_2,...,\mathbf{r}_{N-1};\,t) \times \mathrm{d}\mathbf{r}_2,...,\mathrm{d}\mathbf{r}_{N-1}, \quad (11)$$

which gives

$$\rho_{\rm ion}(\mathbf{r},\,t) = \sum_{\alpha}\left[\sum_{\alpha'\neq\alpha}\gamma_{\alpha'\alpha'}^{(\rm ion)}\right]\varphi_\alpha^2(\mathbf{r}) - \sum_{\alpha}\sum_{\alpha\neq\alpha'}\gamma_{\alpha\alpha'}^{(\rm ion)}\mathrm{e}^{-\mathrm{i}(E_\alpha-E_{\alpha'})t}\varphi_\alpha(\mathbf{r})\varphi_{\alpha'}(\mathbf{r}), \quad (12)$$

where

$$\gamma_{\alpha\alpha'}^{(\rm ion)} = \sum_{lm}\int c_{\alpha\varepsilon lm}(T)c_{\alpha'\varepsilon lm}^{*}(T)\mathrm{d}\varepsilon. \quad (13)$$

The electron density of the neutral molecule does not depend on time in a perturbative approach and is simply given by the sum of the squares of the Kohn–Sham orbitals, $\rho_{\rm neutral}(\mathbf{r}) = \sum_\alpha \varphi_\alpha^2(\mathbf{r})$. The hole density can then be defined as the difference between the electron density of the neutral and the cation, $\rho_{\rm hole}(\mathbf{r},\,t) = \rho_{\rm neutral}(\mathbf{r}) - \rho_{\rm ion}(\mathbf{r},\,t)$, thus also depending on time, and can be expressed in terms of the reduced density matrix of the ion as:

$$\rho_{\rm hole}(\mathbf{r},\,t) = \sum_{\alpha}\left[1-\sum_{\alpha'\neq\alpha}\gamma_{\alpha'\alpha'}^{(\rm ion)}\right]\varphi_\alpha^2(\mathbf{r}) + \sum_{\alpha}\sum_{\alpha\neq\alpha'}\gamma_{\alpha\alpha'}^{(\rm ion)}\mathrm{e}^{-\mathrm{i}(E_\alpha-E_{\alpha'})t}\varphi_\alpha(\mathbf{r})\varphi_{\alpha'}(\mathbf{r}). \quad (14)$$

At any time, one can numerically verify that $\int\rho_{\rm neutral}(\mathbf{r})\mathrm{d}\mathbf{r} = N$, $\int\rho_{\rm ion}(\mathbf{r},\,t)\mathrm{d}\mathbf{r} = N-1$ and $\int\rho_{\rm hole}(\mathbf{r},\,t)\mathrm{d}\mathbf{r} = 1$. Note that the non-diagonal terms in the above expression of the reduced density matrix are non-zero only because the $c_{\alpha\varepsilon lm}$ and $c_{\alpha'\varepsilon lm}$ coefficients have a non-zero value over a large interval of electron energy ε, which makes them overlap in energy. In other words, because the bandwidth of the pulse is larger than the energy separation between different cationic states. For long enough pulses, the above coefficients will have zero overlap in energy and therefore the hole dynamics will be washed out. In general, equations (13) and (14) show that the hole dynamics depends on the pulse characteristics (through the Fourier transform of the pulse), the dipole transition matrix elements (or equivalently the cross sections given in (4) and shown in figure 13) and the orbitals coming into play. In the case of the phenylalanine molecule discussed in previous sections, very delocalized orbitals are involved in the photoionization induced by an ultrashort pulse with the broad bandwidth shown in figure 13. From this figure, we can already expect a non-zero probability of ejecting electrons from any of the 32 orbitals accordingly labeled in figures 12 and 13. The resulting hole is thus expected to be distributed all over the full skeleton of the amino acid as we can see in the snapshots shown in figure 15, where we plot the hole density defined in equation (14) referenced to its average value in time. One can already see charge fluctuations occurring within a few femtoseconds.

The experimental data on phenylalanine and similar amino acids shown in figure 6 in section 3.2 capture the dynamical processes occurring in a temporal scale from a few to tens of femtoseconds, which was already interpreted as the possible signature of ultrafast electron transfer inside the molecule [48]. However, for an accurate study of the electron wave-packet dynamics in the outer-valence molecular orbitals, relevant to most chemical and biological systems, attosecond resolution in the measured observables was required (see [49] and figure 8). In contrast with the vast majority of previous theoretical works and predictions [1, 3, 145, 178], the observed dynamics was not that of a localized hole, but that resulting from the complex wave packet generated by the attosecond pulse. The evolution of such wave packet, resulting from the theoretical calculations described above, is shown in figure 15. From the shown snapshots, it is hard to extract the periodicity of the charge migration events. Therefore, for a better comparison with the experiment, the propagation was extended to longer times in order to later perform a Fourier transform of the signal around a particular atomic center, e.g., around the nitrogen atom. The result is the frequency spectrum shown in the upper panel of figure 16. Looking at figure 14, one might think that most open channels (32 cationic states are energetically open) should be involved in the observed dynamics (since the corresponding ionization cross sections given in figure 13 are similar). However, the frequency spectrum that one would obtain by including all cationic states with identical weights would be that shown in the lower panel of figure 16, which looks like a frequency continuum spectrum rather than a discrete one containing only a few frequencies. This results confirm that a realistic description of the electron dynamics launched by an ultrashort pulse can only be achieved by using the proper ionization amplitudes. Notice that we have focused on the fluctuations around the amino group to compare with the rapid oscillations found in the measured immonium yields in figure 8. This choice was partly consequence of the analysis reported in [48], but also the result of theoretical simulations

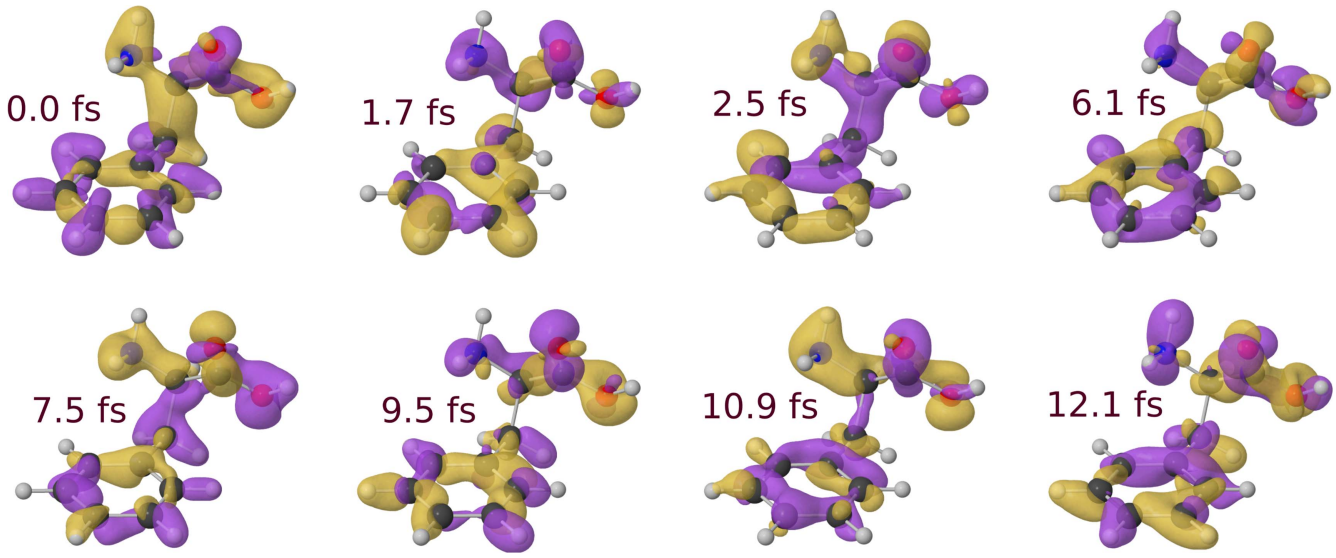


Figure 15. Relative variation of the hole on phenylalanine density with respect to its time-averaged value as a function of time. Isosurfaces of the relative hole density are shown for cutoff values of $+10^{-4}$ (yellow) and -10^{-4} (purple) in arbitrary units. Time is with reference to the end of the XUV pulse (first snapshot).

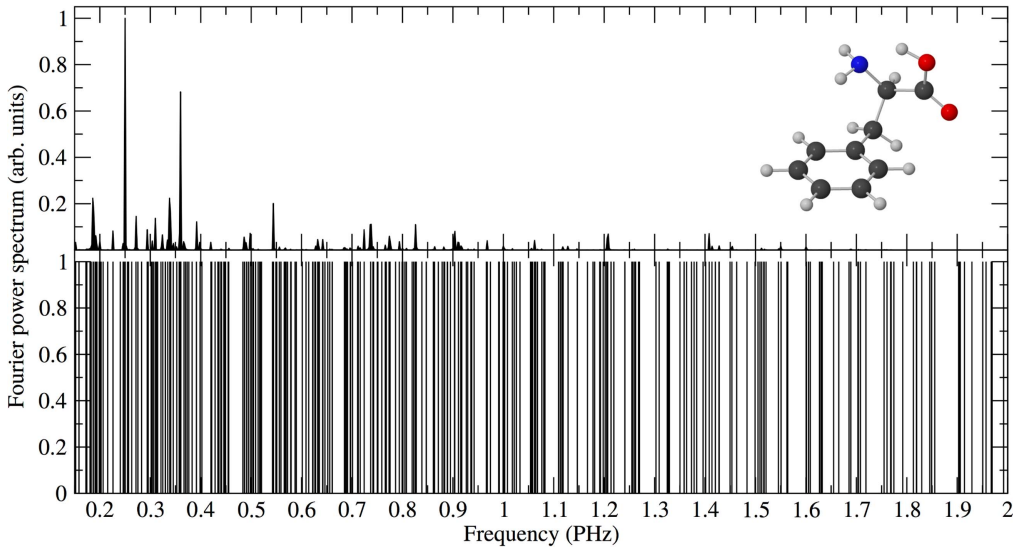


Figure 16. Fourier power spectra of the calculated hole density integrated over the amino group of phenylalanine. Upper panel: results from the actual calculation (as in the upper panel of figure 17). Lower panel: results obtained by using an equal weight for all ionic states accessible by the XUV pulse.

showing that the largest fluctuations are associated to the amino group (see figure 17). In principle one could expect that similar frequency beatings should also show up around other atomic centers of the molecule and, as shown by the Fourier spectra given in figure 17, this is indeed the case. However, there are only two centers leading to significant periodic signals (i.e., large Fourier components): nitrogen and the double bonded oxygen. Since the experiment is capturing immonium fragments, which implies the loss of the carboxyl group, it is thus reasonable to assign the observed beatings to charge fluctuations around the nitrogen atom, since those on the double bonded oxygen atom will be washed out during the separation of the carboxyl group from the rest of the molecule (the immonium dication).

Finally, despite the good agreement obtained for the measured and calculated beating frequencies on the nitrogen atom, it is not clear that similar arguments can be applied to other molecules. Indeed, the experimental observable is the yield of doubly charged immonium ions as a function of the time delay between the XUV attosecond pump and the IR probe, not the time evolution of the density itself. Ideally one should make a direct comparison between theory and experiment for the same observable (challenge (iii) discussed above), namely the immonium yield. Unfortunately, theory is not yet capable of giving a realistic description of the effect of the IR probe pulse nor the subsequent dissociation of the molecular dication after interaction with the IR probe pulse. Thus, one must assume that the dynamics induced by the pump pulse in

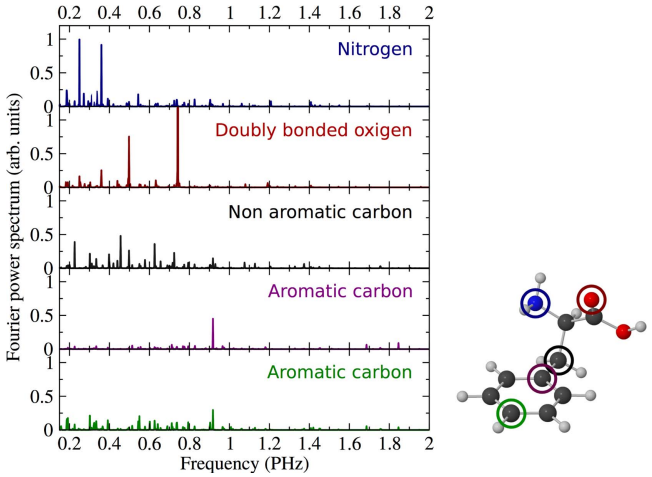


Figure 17. Fourier power spectra of the calculated hole density integrated over various atoms of phenylalanine for the case of randomly oriented molecules. In order to obtain well resolved peaks in frequency, the hole density has been evaluated up to 500 fs.

the singly charged molecule survives in the measured observable. This seems to be a reasonable assumption in view of the good agreement between the measured and calculated frequencies. Furthermore, similar XUV-pump/IR- probe experiments in simpler molecules [11, 40, 52] show that the measured fragmentation yields as a function of time delay indeed contain the signature of the electron dynamics generated by the attosecond pump pulse in the singly charged molecular cation. Nevertheless, further theoretical developments that include the effect of the probe pulse and the ensuing ionization and dissociation of the molecular dication are necessary in order to provide a definitive picture.

6. Conclusions

Scientists are currently pushing the frontiers of attosecond science towards the investigation of electron dynamics in targets of increasing complexity such as biomolecules. The first experimental evidence of charge migration triggered by XUV attosecond pulses in an amino acid has been achieved, and tremendous progress has been made in the theoretical modeling of ultrafast dynamics. Future studies will benefit from the significant developments that are currently taking place in attosecond laser technology (for example at the new European facility ELI-ALPS [197]): on one hand the availability of XUV pulses with higher photon flux (μJ-level) will allow for increasing the time resolution of the experiments by using an XUV-pump XUV-probe scheme; on the other hand, higher-repetition rate sources (hundreds kHz) will open the door to the investigation of even more complex biomolecular targets, which are typically produced in the gas phase with very low density. The disclosure of the role of electrons in the photo-chemistry of bio-relevant molecules will play a key role for understanding, and perhaps even controlling, a number of ultrafast processes of fundamental importance in photo-chemistry and photo-biology.

Acknowledgments

We acknowledge the support from the European Research Council under the ERC grants no. 637756 STARLIGHT, no. 227355 ELYCHE and no. 290853 XCHEM, LASERLAB-EUROPE (grant agreement no. 284464, European Commissions Seventh Framework Programme), European COST Action CM1204 XLIC, the Ministerio de Ciencia e Innovación project FIS2013-42002-R, European grants MC-ITN CORINF and MC-RG ATTOTREND 268284, UKs Science and Technology Facilities Council Laser Loan Scheme, the Engineering and Physical Sciences Research Council (grant EP/J007048/1), the Leverhulme Trust (grant RPG-2012-735), and the Northern Ireland Department of Employment and Learning.

References

[1] Cederbaum L and Zobeley J 1999 *Chem. Phys. Lett.* **307** 205–10
[2] Hennig H, Breidbach J and Cederbaum L S 2005 *J. Phys. Chem.* A **109** 409–14
[3] Remacle F and Levine R D 2006 *Proc. Natl Acad. Sci. USA* **103** 6793–8
[4] Breidbach J and Cederbaum L S 2007 *J. Chem. Phys.* **126** 1–5
[5] Kuleff A I, Lünnemann S and Cederbaum L S 2013 *Chem. Phys.* **414** 100–5
[6] Lépine F, Ivanov M Y and Vrakking M J J 2014 *Nat. Photon.* **8** 195–204
[7] Corkum P B 1993 *Phys. Rev. Lett.* **71** 1994–7
[8] Krausz F and Ivanov M 2009 *Rev. Mod. Phys.* **81** 163–234
[9] Nisoli M and Sansone G 2009 *Prog. Quantum Electron.* **33** 17–59
[10] Chini M, Zhao K and Chang Z 2014 *Nat. Photon.* **8** 178–86
[11] Sansone G, Poletto L and Nisoli M 2010 *Nat. Photon.* **5** 655–63
[12] Fleischer A, Kfir O, Diskin T, Sidorenko P and Cohen O 2014 *Nat. Photon.* **8** 543–9
[13] Kfir O *et al* 2015 *Nat. Photon.* **9** 99–105
[14] Ferré A *et al* 2015 *Nat. Photon.* **9** 93–7
[15] Itatani J, Levesque J, Zeidler D, Niikura H, Pépin H, Kieffer J C, Corkum P B and Villeneuve D M 2004 *Nature* **432** 867–71
[16] Haessler S *et al* 2010 *Nat. Phys.* **6** 200–6
[17] Vozzi C, Negro M, Calegari F, Sansone G, Nisoli M, De Silvestri S and Stagira S 2011 *Nat. Phys.* **7** 822–6
[18] Carpeggiani P, Tzallas P, Palacios A, Gray D, Martìn F and Charalambidis D 2014 *Phys. Rev.* A **89** 023420
[19] Palacios A, González-Castrillo A and Martín F 2014 *Proc. Natl Acad. Sci. USA* **111** 1–6
[20] Corkum P B, Burnett N H and Ivanov M Y 1994 *Opt. Lett.* **19** 1870–2
[21] Tcherbakoff O, Mével E, Descamps D, Plumridge J and Costant E 2003 *Phys. Rev.* A **68** 043804
[22] Sola I J *et al* 2006 *Nat. Phys.* **2** 319–22
[23] Sansone G *et al* 2006 *Science* **314** 443–6
[24] Ferrari F, Calegari F, Lucchini M, Vozzi C, Stagira S, Sansone G and Nisoli M 2010 *Nat. Photon.* **4** 875
[25] Hassan M T *et al* 2016 *Nature* **530** 66–70
[26] Wirth A *et al* 2011 *Science* **334** 195–200
[27] Hassan M T, Wirth A, Grguraš I, Moulet A, Luu T T, Gagnon J, Pervak V and Goulielmakis E 2012 *Rev. Sci. Instrum.* **83** 111301
[28] Nisoli M, De Silvestri S and Svelto O 1996 *Appl. Phys. Lett.* **68** 2793–5

[29] Hentschel M, Kienberger R, Spielmann C, Reider G A, Milosevic N, Brabec T, Corkum P, Heinzmann U, Drescher M and Krausz F 2001 *Nature* **414** 509–13
[30] Itatani J, Quéré F, Yudin G L, Ivanov M Y, Krausz F and Corkum P B 2002 *Phys. Rev. Lett.* **88** 173903
[31] Mairesse Y and Quéré F 2005 *Phys. Rev.* A **71** 011401(R)
[32] Cavalieri A L *et al* 2007 *Nature* **449** 1029–32
[33] Paul P M, Toma E S, Breger P, Mullot G, Augé F, Balcou P, Muller H G and Agostini P 2001 *Science* **292** 1689–92
[34] Dahlström J M, L'Huillier A and Maquet A 2012 *J. Phys. B: At. Mol. Opt. Phys.* **45** 183001
[35] Locher R, Castiglioni L, Lucchini M, Greif M, Gallmann L, Osterwalder J, Hengsberger M and Keller U 2015 *Optica* **2** 405–10
[36] Uiberacker M *et al* 2007 *Nature* **446** 627–32
[37] Sansone G *et al* 2010 *Nature* **465** 763
[38] Trabattoni A *et al* 2015 *Phys. Rev.* X **5** 041053
[39] Kelkensberg F *et al* 2011 *Phys. Rev. Lett.* **107** 043002
[40] Siu W *et al* 2011 *Phys. Rev.* A **84** 063412
[41] Neidel C *et al* 2013 *Phys. Rev. Lett.* **111** 033001
[42] Wang H, Chini M, Chen S, Zhang C H, He F, Cheng Y, Wu Y, Thumm U and Chang Z 2010 *Phys. Rev. Lett.* **105** 143002
[43] Goulielmakis E *et al* 2010 *Nature* **466** 739–44
[44] Ott C *et al* 2014 *Nature* **516** 374–8
[45] Schultze M *et al* 2013 *Nature* **493** 75–8
[46] Schiffrin A *et al* 2013 *Nature* **493** 70–4
[47] Schultze M *et al* 2014 *Science* **346** 1348–52
[48] Belshaw L, Calegari F, Duffy M J, Trabattoni A, Poletto L, Nisoli M and Greenwood J 2012 *J. Phys. Chem. Lett.* **3** 3751
[49] Calegari F *et al* 2014 *Science* **346** 336
[50] Calegari F *et al* 2015 *IEEE JSTQE* **21** 2419218
[51] Kraus P M *et al* 2015 *Science* **350** 790–5
[52] Cörlin P, Fischer A, Schönwald M, Sperl A, Mizuno T, Thumm U, Pfeifer T and Moshammer R 2015 *Phys. Rev.* A **91** 043415
[53] Sandhu A S, Gagnon E, Santra R, Sharma V, Li W, Ho P, Ranitovic P, Cocke C L, Murnane M M and Kapteyn H C 2008 *Science* **322** 1081
[54] Znakovskaya I, von den Hoff P, Zherebtsov S, Wirth A, Herrwerth O, Vrakking M J J, de Vivie-Riedle R and Kling M F 2009 *Phys. Rev. Lett.* **103** 103002
[55] Lucchini M, Kim K, Calegari F, Kelkensberg F, Siu W, Sansone G, Vrakking M J J, Hochlaf M and Nisoli M 2012 *Phys. Rev.* A **86** 043404
[56] Eckstein M, Yang C H, Kubin M, Frassetto F, Poletto L, Ritze H H, Vrakking M J J and Kornilov O 2015 *J. Phys. Chem. Lett.* **6** 419
[57] Marciniak A *et al* 2014 *Nat. Commun.* **6** 1
[58] Lehr L, Horneff T, Weinkauf R and Schlag E W 2005 *J. Phys. Chem.* A **109** 8074–80
[59] Lünnemann S, Kuleff A I and Cederbaum L S 2008 *Chem. Phys. Lett.* **450** 232–5
[60] Boggio-Pasqua M, Groenhof G, Schäfer L V, Grubmüller H and Robb M A 2007 *J. Am. Chem. Soc.* **129** 10996–7
[61] Leo G, Altucci C, Bourgoin-Voillard S, Gravagnuolo A M, Esposito R, Marino G, Costello C E, Velotta R and Birolo L 2013 *Rapid Commun. Mass Spectrom.* **27** 1660–8
[62] Itri F *et al* 2015 *Cell. Mol. Life Sci.* **73** 637–48
[63] Calvert C R *et al* 2012 *Phys. Chem. Chem. Phys.* **14** 6289–97
[64] McPherson A, Gibson G, Jara H, Johann U, Luk T S, McIntyre I A, Boyer K and Rhodes C K 1987 *J. Opt. Soc. Am.* B **4** 595–601
[65] Baker S, Robinson J S, Haworth C A, Teng H, Smith R A, Chirilă C C, Lein M, Tisch J W G and Marangos J P 2006 *Science* **312** 424–7
[66] Kim K T, Villeneuve D M and Corkum P B 2014 *Nat. Photon.* **8** 187–94
[67] Shafir D, Mairesse Y, Villeneuve D M, Corkum P B and Dudovich N 2009 *Nat. Phys.* **5** 412–6
[68] Smirnova O, Mairesse Y, Patchkovskii S, Dudovich N, Villeneuve D, Corkum P and Ivanov M Y 2009 *Nature* **460** 972–7
[69] Shiner A D, Schmidt B E, Trallero-Herrero C, Wörner H J, Patchkovskii S, Corkum P B, Kieffer J C, Légaré F and Villeneuve D M 2011 *Nat. Phys.* **7** 464–7
[70] McFarland B K, Farrell J P, Bucksbaum P H and Gühr M 2008 *Science* **322** 1232–5
[71] Negro M, Devetta M, Faccialà D, De Silvestri S, Vozzi C and Stagira S 2014 *Faraday Discuss.* **171** 133–43
[72] Cireasa R *et al* 2015 *Nat. Phys.* **11** 654–61
[73] Tia M, Cunha de Miranda B, Daly S, Gaie-Levrel F, Garcia G A, Nahon L and Powis I 2014 *J. Phys. Chem.* A **118** 2765–79
[74] Grégoire G 2014 *Nucleic Acids in The Gas Phase* (*Physical Chemistry in Action*) ed V Gebelica (Berlin: Springer)
[75] Taherkhani M, Riese M, BenYezzar M and Müller-Dethlefs K 2010 *Rev. Sci. Instrum.* **81** 063101
[76] Saigusa H, Tomioka A, Katayama T and Iwase E 2006 *Chem. Phys. Lett.* **418** 119–25
[77] Tanaka K 2003 *Angew. Chem. Int. Ed.* **42** 3860–70
[78] Fenn J B 2003 *Angew. Chem. Int. Ed.* **42** 3871–94
[79] Reitsma G *et al* 2014 *Int. J. Mass Spectrom.* **365–366** 365–71
[80] Feraud G, Dedonder C, Jouvet C, Inokuchi Y, Haino T, Sekiya R and Ebata T 2014 *J. Phys. Chem. Lett.* **5** 1236–40
[81] Chatterley A S, West C W, Stavros V G and Verlet J R R 2014 *Chem. Sci.* **5** 3963–75
[82] Mooney C R S, Horke D A, Chatterley A S, Simperler A, Fielding H H and Verlet J R R 2013 *Chem. Sci.* **4** 921–7
[83] Gaie-Levrel F, Garcia G A, Schwell M and Nahon L 2011 *Phys. Chem. Chem. Phys.* **13** 7024–36
[84] Morgner N, Barth H D and Brutschy B 2006 *Aust. J. Chem.* **59** 109–14
[85] Charvet A and Abel B 2007 *Phys. Chem. Chem. Phys.* **9** 3335–60
[86] Berkowitz J and Chupka W A 1965 *Chem. Phys.* **40** 2735–6
[87] Lincoln K A 1965 *Anal. Chem.* **37** 541–3
[88] Tanaka K, Wadi H, Ido Y, Akita S and Yoshida T 1988 *Commun. Mass Spectrom.* **2** 151–3
[89] Hall R B 1987 *J. Phys. Chem.* **91** 1007–15
[90] Levis R J 1994 *Annu. Rev. Phys. Chem.* **45** 483–518
[91] Wei J, Buriak J M and Siuzdak G 1999 *Nature* **399** 243–6
[92] Arakawa R and Kawasaki H 2010 *Anal. Sci.* **26** 1229–40
[93] Levy D H 1980 *Annu. Rev. Phys. Chem.* **31** 197–225
[94] Levy D H 1981 *Science* **214** 263–9
[95] Cable J R, Tubergen M J and Levy D H 1987 *J. Am. Chem. Soc.* **109** 6198–9
[96] Grotemeyer J, Boesl U, Walter K and Schlag E W 1987 *Anal. Instrum.* **16** 151–71
[97] Li L and Lubman D M 1988 *Rev. Sci. Instrum.* **59** 557–61
[98] Arrowsmith P, de Vries M S, Hunziker H E and Wendt H R 1988 *AIP Conf. Proc.* **172** 770–2
[99] Meijer G, de Vries M S, Hunziker H E and Wendt H R 1990 *Appl. Phys.* B **51** 395–403
[100] Knochenmuss R 2006 *Analyst* **131** 966
[101] Chang W C, Huang L C L, Wang Y-S, Peng W-P, Chang H C, Hsu N Y, Yang W B and Chen C H 2007 *Anal. Chim. Acta* **582** 1–9
[102] Allwood D A, Dyer P E, Dreyfus R W and Perera I K 1997 *Appl. Surf. Sci.* **109/110** 616–20
[103] Merrigan T L, Hunniford C A, Timson D J, Morrow T, Catney M and McCullough R W 2008 *J. Phys. Conf. Ser.* **101** 012016
[104] Lindner B and Seydel U 1985 *Anal. Chem.* **57** 895–9
[105] Golovlev V V, Allman S L, Garrett W R, Taraneko N I and Chen C H 1997 *Int. J. Mass Spectrom.* **169** 69–78

[106] Pérez J, Ramírez-Arizmendi L E, Petzold C J, Guler L P, Nelson E D and Kenttäma H I 2000 *Int. J. Mass Spectrom.* **198** 173–88
[107] Shea R C, Petzold C J, Campbell J L, Sen L, Aaserud D J and Kenttäma H I 2006 *Anal. Chem.* **78** 6133–9
[108] Shea R C, Habicht S C, Vaughn W E and Kenttäma H I 2007 *Anal. Chem.* **79** 2688–94
[109] Zinovev A V, Veryovkin I V, Moore J F and Pellin M J 2007 *Anal. Chem.* **79** 2688–94
[110] Nyadong L, McKenna A M, Hendrickson C L, Rodgers R P and Marshall A G 2011 *Anal. Chem.* **83** 1616–23
[111] Duffy M J *et al* 2013 *J. Am. Soc. Mass Spectrom.* **24** 1366–75
[112] Sezer U, Wörner L, Horak J, Felix L, Tüxen J, Götz C, Vaziri A, Mayor M and Arndt M 2015 *Anal. Chem.* **87** 5614–9
[113] Zinovev A, Veryovkin I and Pellin M 2011 Molecular desorption by laser-driven acoustic waves: analytical applications and physical mechanisms *Acoustic Waves—From Microdevices to Helioseismology* ed M G Beghi (Rijeka (HRV): InTech) ISBN: 978-953-307-572-3
[114] Greenwood J B, Miles J, De Camillis S, Mulholland P, Zhang L, Parkes M A, Hailes H C and Fielding H H 2014 *J. Phys. Chem. Lett.* **5** 3588–92
[115] Poully J-C, Miles J, De Camillis S, Cassimi A and Greenwood J B 2015 *Phys. Chem. Chem. Phys.* **17** 7172–80
[116] De Camillis S, Miles J, Alexander G, Ghafur O, Williams I D, Townsend D and Greenwood J B 2015 *Phys. Chem. Chem. Phys.* **17** 23643–50
[117] Adamson B D, Coughlan N J A, Markworth P B, Continetti R E and Bieske E J 2014 *Rev. Sci. Instrum.* **85** 123109
[118] Lee K T, Sung J, Lee K J, Kim S K and Park Y D 2002 *J. Chem. Phys.* **116** 8251–4
[119] Rizzo T R, Park Y D, Peteanu L A and Levy D H 1986 *J. Chem. Phys.* **84** 2534–41
[120] Martinez S J, Alfano J C and Levy D H 1992 *J. Mol. Spectrosc.* **156** 421–30
[121] Filsinger F, Erlekam U, von Helden G, Küpper J and Meijer G 2008 *Phys. Rev. Lett.* **100** 133003
[122] van de Meerakker S Y T, Bethlem H L, Vanhaecke N and Meijer G 2012 *Chem. Rev.* **112** 4828–78
[123] Filsinger F, Küpper J, Meijer G, Hansen J L, Maurer J, Nielsen J H, Holmegaard L and Stapelfeldt H 2009 *Angew. Chem. Int. Ed.* **48** 6900–2
[124] Kierspel T, Horke D A, Chang Y-P and Küpper J 2014 *Chem. Phys. Lett.* **591** 130–2
[125] Huang Z, Yu W and Lin Z 2006 *J. Mol. Struct. THEOCHEM* **758** 195–202
[126] Drescher M, Hentschel M, Kienberger R, Uiberacker M, Yakovlev V, Scrinzi A, Westerwalbesloh T, Kleineberg U, Heinzmann U and Krausz F 2002 *Nature* **419** 803–7
[127] Kienberger R *et al* 2002 *Science* **297** 1144–8
[128] Baltuška A *et al* 2003 *Nature* **421** 611–5
[129] Mauritsson J, Johnsson P, Mansten E, Swoboda M, Ruchon T, LHuillier A and Schafer K J 2008 *Phys. Rev. Lett.* **100** 073003
[130] Niikura H, Légaré F, Hasbani R, Bandrauk a D, Ivanov M Y, Villeneuve D M and Corkum P B 2002 *Nature* **417** 917–22
[131] Ranitovic P *et al* 2014 *Proc. Natl Acad. Sci.* **111** 912–7
[132] Leone S R *et al* 2014 *Nat. Photon.* **8** 162–6
[133] Golubev N V and Kuleff A I 2015 *Phys. Rev.* A **91** 1–5
[134] Calvert C, Bryan W, Newell W and Williams I 2010 *Phys. Rep.* **491** 1–28
[135] Palacios A, Sanz-Vicario J L and Martín F 2015 *J. Phys. B: At. Mol. Opt. Phys.* **48** 242001
[136] Caillat J, Zanghellini J, Kitzler M, Koch O, Kreuzer W and Scrinzi A 2005 *Phys. Rev.* A **71** 012712
[137] Koch O, Kreuzer W and Scrinzi A 2006 *Appl. Math. Comput.* **173** 960–76
[138] Kato T and Kono H 2008 *J. Chem. Phys.* **128** 184102
[139] Kato T and Yamanouchi K 2009 *J. Chem. Phys.* **131** 164118
[140] Alon O, Streltsov A and Cederbaum L 2009 *Phys. Rev.* A **79** 022503
[141] Nest M 2009 *Chem. Phys. Lett.* **472** 171–4
[142] Haxton D J, Lawler K V and McCurdy C W 2011 *Phys. Rev.* A **83** 063416
[143] Haxton D J and McCurdy C W 2014 *Phys. Rev.* A **90** 053426
[144] Haxton D J and McCurdy C W 2015 *Phys. Rev.* A **91** 012509
[145] Kuleff A I and Cederbaum L S 2014 *J. Phys. B: At. Mol. Opt. Phys.* **47** 124002
[146] Pabst S, Greenman L, Ho P J, Mazziotti D A and Santra R 2011 *Phys. Rev. Lett.* **106** 053003
[147] Lischka H *et al* Columbus, an ab initio electronic structure program, release 7.0 http://univie.ac.at/columbus/accessed (accessed 2015)
[148] Computing A S and Modeling Vrije universiteit Amsterdam, Netherlands www.scm.com
[149] Andreoni W and Curioni A 2000 *Parallel Comput.* **26** 819–842
[150] Aidas K *et al* 2014 The Dalton quantum chemistry program system *Comput. Mol. Sci.* **4** 269–84
[151] Furche F, Ahlrichs R, Hättig C, Klopper W, Sierka M and Weigend F 2014 *WIREs Comput. Mol. Sci.* **4** 91–100
[152] Aquilante F *et al* 2010 *J. Comput. Chem.* **31** 224–47
[153] Werner H-J, Knowles P J, Knizia G, Manby F R and Schütz M 2012 *WIREs Comput. Mol. Sci.* **2** 242–53
[154] Guest M, Bush I J, van DamH, Sherwood P, Thomas J, van Lenthe J, Havenith R and Kendrick J 2005 The gamess-UK electronic structure package: algorithms, developments and applications *Mol. Phys.* **103** 719–47
[155] Frisch M J *et al* 2009 Gaussian09 Revision D.01 (Wallingford, CT: Gaussian Inc.)
[156] Valiev M *et al* 2010 http://nwchem-sw.org
[157] Cooper B, Kolorenč P, Frasinski L J, Averbukh V and Marangos J P 2014 *Faraday Discuss.* **171** 93–111
[158] Kuleff A I, Breidbach J and Cederbaum L S 2005 *J. Chem. Phys.* **123** 044111
[159] Kuleff A I and Cederbaum L S 2007 *Chem. Phys.* **338** 320–8
[160] Mignolet B, Levine R D and Remacle F 2014 *J. Phys. B: At. Mol. Opt. Phys.* **47** 124011
[161] Pickup B T 1977 *Chem. Phys.* **19** 193–208
[162] Öhrn Y and Born G 1981 *Adv. Quantum Chem.* **13** 1–88
[163] Stratmann R E, Bandarage G and Lucchese R R 1995 *Phys. Rev.* A **51** 3756–65
[164] Stratmann R E, Zurales R W and Lucchese R R 1996 *J. Chem. Phys.* **104** 8989–9000
[165] Rescigno T N, Lengsfield B H and Orel A E 1993 *J. Chem. Phys.* **99** 5097–103
[166] Rescigno T N, Lengsfield B H and McCurdy C W 1995 *Adv. Ser. Phys. Chem.* **1** 501
[167] Rescigno T N, Trevisan C S and Orel A E 2015 *Phys. Rev.* A **99** 023429
[168] Toffoli M D, Stener G F and Decleva P 2002 *Chem. Phys.* **276** 25–43
[169] Stener M, Furlan S and Decleva P 2000 *J. Phys. B: At. Mol. Opt. Phys.* **33** 1081
[170] Stener M, Fronzoni G and Decleva P 2005 *J. Chem. Phys.* **122** 234301
[171] Toffoli D, Stener M, Fronzoni G and Decleva P 2006 *J. Chem. Phys.* **124** 214313
[172] Carroll T X, Zahl M G, Brve K J, Sthre L J, Decleva P, Ponzi A, Kas J J, Vila F D, Rehr J J and Thomas T D 2013 *J. Chem. Phys.* **138** 234310

[173] Kushawaha R K, Patanen M, Guillemin R, Journel L, Miron C, Simon M, Piancastelli M N, Skates C and Decleva P 2013 *Proc. Natl Acad. Sci.* **110** 15201–6
[174] Mignolet B, Levine R D and Remacle F 2012 *Phys. Rev.* A **86** 1–8
[175] Breidbach J and Cederbaum L S 2003 *J. Chem. Phys.* **118** 3983
[176] Breidbach J and Cederbaum L S 2005 *Phys. Rev. Lett.* **94** 033901
[177] Despré V, Marciniak A, Loriot V, Galbraith M C E, Rouzée A, Vrakking M J J, Lépine F and Kuleff A I 2015 *J. Phys. Chem. Lett.* **6** 426–31
[178] Vacher M, Bearpark M and Robb M 2014 *J. Chem. Phys.* **140** 201102
[179] Vacher M, Steinberg L, Jenkins A J, Bearpark M J and Robb M A 2015 *Phys. Rev.* A **92** 040502
[180] Canton S E, Plesiat E, Bozek J D, Rude B S, Decleva P and Martin F 2011 *Proc. Natl Acad. Sci.* **108** 7302–6
[181] Plésiat E, Argenti L, Kukk E, Miron C, Ueda K, Decleva P and Martín F 2012 *Phys. Rev.* A **85** 023409
[182] Kukk E *et al* 2013 *Phys. Rev.* A **88** 033412
[183] Ayuso D, Palacios A, Decleva P and Martín F 2013 *J. Electron Spectrosc. Relat. Phenom.* **195** 320–6
[184] Argenti L *et al* 2012 *New J. Phys.* **14** 033012
[185] Ueda K *et al* 2013 *J. Chem. Phys.* **139** 124306
[186] Ayuso D *et al* 2015 *J. Phys. Chem.* A **119** 5971–8
[187] Stener M, Lisini A and Decleva P 1995 *Int. J. Quantum Chem.* **53** 229–44
[188] Stener M and Decleva P 2000 *J. Chem. Phys.* **112** 10871–9
[189] van Leeuwen R and Baerends E J 1994 *Phys. Rev.* A **49** 2421–31
[190] Lee C, Yang W and Parr R G 1988 *Phys. Rev.* B **37** 785–9
[191] Becke A D 1993 *J. Chem. Phys.* **98** 5648–52
[192] Csaszar A G 1992 *J. Am. Chem. Soc.* **114** 9568–75
[193] Snoek L C, Kroemer R T, Hockridge M R and Simons J P 2001 *Phys. Chem. Chem. Phys.* **3** 1819–26
[194] te Velde G, Bickelhaupt F M, Baerends E J, Fonseca Guerra C, van Gisbergen S J A, Snijders J G and Ziegler T 2001 *J. Comput. Chem.* **22** 931–67
[195] Fischer C F and Idrees M 1990 *J. Phys. B: At. Mol. Opt. Phys.* **23** 679
[196] Bachau H, Cormier E, Decleva P, Hansen J E and Martín F 2001 *Rep. Prog. Phys.* **64** 1815
[197] ELI-ALPS http://eli-hu.hu